Computer Modeling in Engineering & Sciences

Tech Science Press

Doi:10.32604/cmes.2025.069541

ARTICLE

Predictive and Global Effect of Active Smoker in Asthma Dynamics with Caputo Fractional Derivative

Muhammad Farman[1,2,3,*], Noreen Asghar[4], Muhammad Umer Saleem[4], Kottakkaran Sooppy Nisar[5,6], Kamyar Hosseini[1,2,7] and Mohamed Hafez[8,9]

[1]Faculty of Arts and Sciences, Department of Mathematics, Near East University, TRNC, Mersin 10, Nicosia, 99138, Turkey
[2]Research Center of Applied Mathematics, Khazar University, Baku, AZ-1096, Azerbaijan
[3]Jadara University Research Center, Jadara University, Irbid, 21110, Jordan
[4]Department of Mathematics, University of Education, Lahore, 54600, Pakistan
[5]Department of Mathematics, College of Science and Humanities in Al Kharj, Prince Sattam bin Abdulaziz University, Al Kharj, 16277, Saudi Arabia
[6]Hourani Center for Applied Scientific Research, Al-Ahliyya Amman University, Amman, 19328, Jordan
[7]Faculty of Engineering and Natural Sciences, Istanbul Okan University, Istanbul, 34959, Turkey
[8]Faculty of Engineering and Quantity Surveying, INTI International University Colleges, Nilai, 71800, Malaysia
[9]Faculty of Mangement, Shinawatra University, Pathum Thani, 12000, Thailand

*Corresponding Author: Muhammad Farman. Email: farmanlink@gmail.com

Received: 25 June 2025; Accepted: 03 September 2025; Published: 30 October 2025

ABSTRACT: Smoking is harmful to the lungs and has numerous effects on our bodies. This leads to decreased lung function, which increases the lungs' susceptibility to asthma triggers. In this paper, we develop a new fractional-order model and investigate the impact of smoking on the progression of asthma by using the Caputo operator to analyze different factors. Using the Banach contraction principle, the existence and uniqueness of solutions are established, and the positivity and boundedness of the model are proved. The model further incorporates different stages of smoking to account for incubation periods and other latent effects, enhancing the accuracy of system dynamics. Within this Fractional operator framework, key analyses are performed, including the identification of equilibrium points, computation of the basic reproduction number, sensitivity analysis, and assessment of local and global stability with the Lyapunov function. Additionally, chaos stability employing linear response regulation is implemented mathematically, and the effect of the compartment shows through simulations. A numerical iterative method employing Newton polynomial interpolation is used to illustrate the effectiveness of the suggested model, and numerical simulations reveal its enhanced efficiency at various fractional orders. The fractional-order framework offers a more realistic representation than classical integer-order models.

KEYWORDS: Smoking-induced asthma; health risk control; chaos stability; biological algorithm; computational analysis

1 Introduction

Asthma is a chronic disease that causes difficulty breathing by affecting the inner walls of the airways. Breathing difficulties and shortness of breath when exhaling are symptoms of the chronic illness asthma. Although there is no particular treatment, symptoms can be tracked. Patients should speak with medical professionals who can modify their treatment according to the patient's condition. Chest tightness, discomfort, coughing, wheezing, respiratory system infections, dyspnea, and trouble sleeping are some of the symptoms.

Children with asthma frequently exhibit wheezing during exhalation, which causes breathing problems. Asthmatic patients may have severe symptoms such as chest pain and loss of consciousness due to a shortage of oxygen.

According to reports, cigarette smoke can also cause asthma in addition to air pollutants such hexachloroplatinates and di-isocynates [1–3]. Smoking is harmful to the lungs and has numerous effects on our bodies. This leads to decreased lung function, which increases the lungs' susceptibility to asthma triggers. Cigarette smoke contains high levels of irritants such as formaldehyde, ammonia, acrolein, and nitrogen oxides. The expert maintained that smoke which enter the host through a close smoker in the community, can harm the lungs. As a result, when someone inhales tobacco smoke, these disagreeable chemicals may trigger an asthma attack. Over 1,000,000 children with asthma worsen after being exposed to secondhand smoke, and over 15 million children are exposed to smoke every day [4,5]. Asthma is also caused by airborne pollutants, including dust from open-pit coal mining, coal-fired cement, and other operations, heavy metal cocktails from Solid Liquid Fuel (SLF) burning cement, and vanadium and nickel particles from power plants and oil refineries [6–8]. As a result, a susceptible population develops asthma as a result of ongoing exposure to air pollutants. To investigate the patterns of transmission of infectious diseases [9–12] and generate vital data regarding disease dynamics for control and prevention [13,14], mathematical models are crucial. Researchers have created a variety of numerical techniques to study disease dynamics. Researchers have recently examined the dynamics of asthma from a variety of angles in their study [15,16]. It is well known that ongoing smoking exposure is a major factor in the onset and progression of asthma.

Because fractional calculus is inherited and uses memory-based depictions, it is a flexible framework that provides accurate results in science and technology [17–19]. Using its derivative for a constant being zero, Caputo's fractional derivative enables the solution of problems using conventional beginning and boundary conditions [20–22]. Nonlinear functional integral equations can now be solved with a variety of fractional operators (see [23,24]) thanks to new advances in fractional calculus. Dinku et al. [25] used various kernels of fractional differential equations to examine the effect of smoking on the development of cancer. To take into consideration the periodic impacts of smoking, they included a periodic function. For a variety of fractional-order derivatives, the study examined chaotic behavior, such as high smoking frequency and absence of immunological flux under low host cell starting circumstances. The goal of the study [26] was to compare the outcomes with conventional models by using fractional calculus to investigate adsorption and extraction processes. Equations were solved using the Caputo derivative, and processes such as the extraction of maize antioxidant compounds with varying solvent amounts and the adsorption of biodiesel glycerol at varying temperatures were examined. First-order and So and MacDonald's models were used to compare the extraction of antioxidant chemicals. The diagnosis and therapy of lung cancer in patients with compromised immune systems utilizing cytokines and anti-PD-L1 inhibitors was investigated by Nisar et al. [27]. In addition to identifying early lung cancer management by cytokines and anti-PD-L1 inhibitors, which promote the generation of anti-cancer cells, they verified immune-mediated compartment linkages. IABNs were developed by Mukhtar et al. [28] to solve fractional order Parkinson's disease scenarios. Through evaluations with regard numerical solutions and simulations, the IABN was examined. An excellent method for forecasting significant deformations of amorphous polymers is the variable order fractional parametric model, which was refined in [29]. It characterizes the mechanical behavior of polycarbonate at various temperatures. Using a fractional-order system, Farman et al. [30] demonstrate how decreased resources from forests affect toxin activity and fire caused by humans. These steps are intended to confirm that resource depletion has been resolved. In ecological modeling, fractional calculus is crucial for comprehending and overseeing maintaining forests in the face of human pressures, according to the study. Using GA, Adak et al. [31] optimized a SIR fractional order model that included medication, the media, and vaccine controls.

The order of fractional derivatives was shown to affect the ideal management parameter values. The fractional operator in the Caputo sense was used by Bansal et al. [32] to create a mathematical model for studying the dynamics of transmitting monkeypox in both humans and other species.

Traditional integer-order differential equations have been widely used to model the dynamics of asthma and its association with environmental pollutants, including tobacco smoke [33]. Incidents of asthma are closely related to environmental variables such as smoking, pollution in the air, and allergens. However, breathing difficulties can be reduced with medication-based therapy and limiting exposure to asthma triggers. Recent advancements have introduced fractional-order derivatives to better capture memory effects and hereditary properties inherent in biological systems [34,35]. Inspired by the debate above, we create a novel model in this work to examine the dynamics of different smoker classes that have the potential to spread asthma. As far as we are aware, this effort is novel and will investigate further perspectives on the problem. Furthermore, because fractional-order models better capture the intricate physical processes, we used the Caputo fractional operator rather than integer-order. The investigation of dynamical behavior throughout the entire time span and its precise mathematical characterization are currently the main challenges. The intricate dynamical processes found in smoking-induced asthma disease can be better described by fractional-order models.

The structure of this manuscript is as follows: A brief description of the fractional operator utilized in the suggested model is given in Section 2. The fractional-order-based smoking-induced asthma model is the main topic of Section 3, and a thorough examination of the generated model is included in Section 4. Section 5 explores the system's stability using the Lyapunov stability approach. Inside the practicable spectrum, Section 6 examines the model's performance under chaotic circumstances; Section 7 displays the numerical outcomes derived from the system; Section 8 supplies an in-depth analysis of the outcomes, and delivers a summary of the most significant results and the ultimate findings.

2 Formulation of Dynamical Model for Smoking-Induced Asthma

In this work, we developed a new model of smoking-induced asthma disease flow chart shown in Fig. 1. Smokers are divided into three classes as:

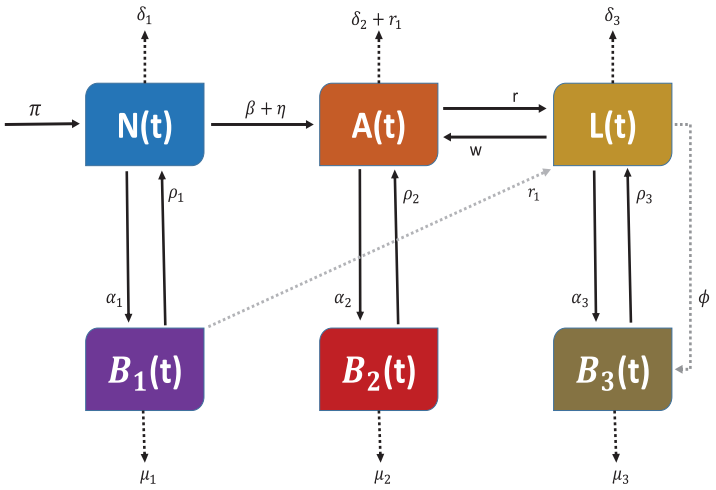

Figure 1: The flow chart of dynamical system

- $N(t)$; Non-smoker class;
- $A(t)$: Active-smoker class; and

- $L(t)$: Ex-smoker class.

Smoking-induced asthma population is categorized as follows:

- $B_1(t)$: Asthma diagnose due to non-smoker class;
- $B_2(t)$: Asthma diagnose due to active-smoker class; and
- $B_3(t)$: Asthma diagnose due to ex-smoker class.

2.1 Assumptions

- π represents the non-smokers $N(t)'$ recruiting rate, while δ_1 represents the natural death rate. We assumed that the number of nonsmokers would decline when they begin to smoke at a rate of β and as a result of outside influences at a rate of η. Additionally, nonsmokers spread asthma at a rate of α_1, and the number of nonsmokers who recover from asthma also contributes to the class $N(t)$. Thus at time t, we have

$$N(t) = \pi - (\beta + \eta)N - \alpha_1 N - \delta_1 N + \rho_1 B_1. \tag{1}$$

- Active smokers $A(t)$ increase at the rate of β and η, and also with the temporary improvement rate of w due to ex-smokers. The number of active smokers decrease due to natural death rate of δ_2, naturally smoking-quit rate of r, and as well as due to asthma at the rate of r_1. Moreover, $A(t)$ spread asthma at a rate of α_2 and they decrease as they recover from asthma at a rate of ρ_2. Therefore,

$$A(t) = (\beta + \eta)N + wL - (r + r_1)A - (\alpha_2 + \delta_2)A + \rho_2 B_2. \tag{2}$$

- The class $L(t)$ of ex-smokers rises at a smoking-quit rate of r and a quit rate of r_1 because of asthma. Due to the recovered ex-smokers, the number of $L(t)$ also rises at a rate of ρ_3. The transmission rates of asthma and natural death, represented by α_3 and δ_3, respectively, cause a drop in the number of $L(t)$.

$$L(t) = rA + r_1 B_1 - (\alpha_3 + \delta_3 - w)L + \rho_3 B_3. \tag{3}$$

- The class $B_1(t)$ increases when ex-smokers $(L(t))$ come into contact with asthma and transmit it at a rate of α_1. $B_1(t)$ class decreases as per natural death rate (μ_1) and the recovery rate (ρ_1) of active smokers having asthma.

$$B_1(t) = \alpha_1 N - (\rho_1 + \mu_1)B_1. \tag{4}$$

- The class $B_2(t)$ increases when active smokers $(A(t))$ come into contact with asthma and transmit it at a rate of α_2. $B_3(t)$ class reduces due to the natural death rate (μ_2) and the recovery rate (ρ_2) of active smokers having asthma.

$$B_2(t) = \alpha_2 A - (\rho_2 + \mu_2)B_2. \tag{5}$$

- The class $B_3(t)$ increases when ex-smokers $(L(t))$ come into contact with asthma and transmit it at a rate of α_3. It also increases due to certain external impacts indicated by ϕ. $B_3(t)$ class falls due to the natural death rate (μ_3) and the recovery rate (ρ_3) of ex-smokers having asthma.

$$B_3(t) = \alpha_3 L + \phi B_3 - (\rho_3 + \mu_3)B_3. \tag{6}$$

2.2 Fractional-Order Model

A variable's rate of change in classical modeling using ordinary differential equations is entirely dependent on its existing state. These models' basic presumption that the system is memoryless restricts

their capacity to represent biological processes impacted by prior actions. The Caputo fractional-order derivative presents a memory-dependent paradigm in which the system's current state is impacted by every condition in the past via a weighted history. This characteristic is especially crucial for long-term respiratory disorders like asthma, where the effects of environmental exposures, like smoking, take time to manifest. Because the Caputo operator makes the switch from classical to fractional modeling more natural by allowing the integration of beginning conditions in the same form as classical derivatives, it is particularly well-suited for modeling such memory effects. A more realistic depiction of the disease's course is achieved by incorporating the memory feature into the model, which successfully captures inflammatory accumulation, delayed immune responses, and residual smoking-related harm. Therefore, in comparison to conventional Ordinary Differential Equations (ODEs), the fractional-order model with the Caputo derivative offers a more thorough and biologically compatible approach.

There are numerous uses for fractional calculus. In contrast to other derivatives of non-integer orders, the Caputo fractional derivative is a fundamental idea in fractional calculus that finds practical tractability in problem modeling, providing rich and precise information. A possible physical manifestation of real-life phenomena, such the memory of smoking-induced asthma that explains a system's behavior in the past, is the arbitrary fractional order. Here, we are discussing some fundamental findings that are essential to our work.

Definition 1. *[36] For a continuous function $\Psi(t)$, the Riemann-Liouville integral definition of order θ is:*

$$ {}_0^R I_t^\theta \Psi(t) = \frac{1}{\Gamma(\theta)} \int_0^t (t-\tau)^{(\theta-1)} \Psi(\tau) d\tau. \tag{7} $$

Definition 2. *[36] The Caputo derivative operator of order θ can be written as:*

$$ {}_0^C D_t^\theta \Psi(t) = \frac{1}{\Gamma(m-\theta)} \left[\int_0^t (t-\tau)^{m-\theta-1} \Psi'(t)(\tau) d\tau \right], \tag{8} $$

where $m = [\theta]$ is the smallest integer and $m-1 < \theta < m$.

Consequently, by improving the data fitting versatility, the fractional order parameter makes it possible to describe the asthma disease system using the Caputo derivative structure in an extra adaptable way.

$$ \begin{aligned} {}^C D_t^\theta N(t) &= \pi - (\beta+\eta)N - \alpha_1 N - \delta_1 N + \rho_1 B_1, \\ {}^C D_t^\theta A(t) &= (\beta+\eta)N + wL - (r+r_1)A - (\alpha_2+\delta_2)A + \rho_2 B_2, \\ {}^C D_t^\theta L(t) &= rA + r_1 B_1 - (\alpha_3+\delta_3-w)L + \rho_3 B_3, \\ {}^C D_t^\theta B_1(t) &= \alpha_1 N - (\rho_1+\mu_1)B_1, \\ {}^C D_t^\theta B_2(t) &= \alpha_2 A - (\rho_2+\mu_2)B_2, \\ {}^C D_t^\theta B_3(t) &= \alpha_3 L + \phi B_3 - (\rho_3+\mu_3)B_3, \end{aligned} \tag{9} $$

with initial condition $N(0) \geq 0$, $A(0) \geq 0$, $L(0) \geq 0$, $B_1(0) \geq 0$, $B_2(0) \geq 0$, $B_3(0) \geq 0$. Here, θ is the order of Caputo fractional derivative $({}^C D_t)$ such that $0 < \theta \leq 1$.

2.3 Positiveness and Boundedness of Solutions

In this part, we find the conditions ensuring the poistivity of the solutions, which are crucial for representing real-world scenarios. For $N(t)$, we have

$$\begin{aligned} {}^{C}D_t^{\theta}N(t) &= \pi - (\beta+\eta)N - \alpha_1 N - \delta_1 N + \rho_1 B_1, \\ &\geq -(\beta+\eta+\alpha_1+\delta_1)N. \end{aligned} \tag{10}$$

This holds for all $t \geq 0$ when considering classical derivatives.

$$N(t) \geq N(0)e^{-(\beta+\eta+\alpha_1+\delta_1)t}. \tag{11}$$

Notably, when dealing with classical derivatives, these properties hold for all $t \geq 0$.

$$\begin{aligned} &A(t) \geq A(0)e^{-(r+r_1+\alpha_2+\delta_2)t}, \\ &L(t) \geq L(0)e^{-(\alpha_3+\delta_3-w)t}, \\ &B_1(t) \geq B_1(0)e^{-(\rho_1+\mu_1)t}, \\ &B_2(t) \geq B_2(0)e^{-(\rho_2+\mu_2)t}, \\ &B_3(t) \geq B_3(0)e^{-(\rho_3+\mu_3-\phi)t}. \end{aligned} \tag{12}$$

While the positivity of system solutions in terms of Caputo derivative is defined by

$$\begin{aligned} &N(t) \geq N(0)\Lambda_{\theta}\big[-(\beta+\eta+\alpha_1+\delta_1)t^{\theta}\big], \\ &A(t) \geq A(0)\Lambda_{\theta}\big[-(r+r_1+\alpha_2+\delta_2)t^{\theta}\big], \\ &L(t) \geq L(0)\Lambda_{\theta}\big[-(\alpha_3+\delta_3-w)t^{\theta}\big], \\ &B_1(t) \geq B_1(0)\Lambda_{\theta}\big[-(\rho_1+\mu_1)t^{\theta}\big], \\ &B_2(t) \geq B_2(0)\Lambda_{\theta}\big[-(\rho_2+\mu_2)t^{\theta}\big], \\ &B_3(t) \geq B_3(0)\Lambda_{\theta}\big[-(\rho_3+\mu_3-\phi)t^{\theta}\big]. \end{aligned} \tag{13}$$

2.4 Positively Invariant Region

Lemma 1. *For the remainder of the time span, assuming the nonnegative starting conditions, the solutions of the system (9) remain in the confined positive region* R_{+}^{6}.

Proof. We obtain the following:

$$\begin{aligned} &{}^{C}D_t^{\theta}N(t)\,|_{N=0} = \pi + \rho_1 B_1 \geq 0, \\ &{}^{C}D_t^{\theta}A(t)\,|_{A=0} = (\beta+\eta)N + wL + \rho_2 B_2 \geq 0, \\ &{}^{C}D_t^{\theta}L(t)\,|_{L=0} = rA + r_1 B_1 + \rho_3 B_3 \geq 0, \\ &{}^{C}D_t^{\theta}B_1(t)\,|_{B_1=0} = \alpha_1 N \geq 0, \\ &{}^{C}D_t^{\theta}B_2(t)\,|_{B_2=0} = \alpha_2 A \geq 0, \\ &{}^{C}D_t^{\theta}B_3(t)\,|_{B_3=0} = \alpha_3 L \geq 0. \end{aligned} \tag{14}$$

Now, we sum up the all equations in (9). Then we obtain

$$\begin{aligned} M(t) &= \pi - \delta_1 N + (w - r_1 - \delta_2)A + (2w - \delta_3)L + (r_1 - \mu_1)B_1 - \mu_2 B_2 + (\phi - \mu_3)B_3, \\ &\geq \pi - \kappa M. \end{aligned} \tag{15}$$

This yields

$$\lim_{t\to\infty} SupM(t) \leq \frac{\pi}{\kappa}. \tag{16}$$

Thus, we can conclude that

$$\Upsilon = \left((N, A, L, B_1, B_2, B_3) \in \mathrm{R}_+^6 : 0 \leq M(t) \leq \frac{\pi}{\kappa} \right), \tag{17}$$

is a positively invariant region.□

2.5 Equilibrium Points

By setting the system's left side to zero, this part offers a thorough examination of equilibrium locations. Let there are no active smokers and in the absence of asthma we get the points free of disease as

$$\begin{aligned} E^0 &= \left(N^0,\ A^0,\ L^0,\ B_1^0,\ B_2^0,\ B_3^0\right), \\ &= \left(\frac{\pi}{(\beta + \eta + \alpha_1 + \delta_1)}, 0, 0, 0, 0, 0 \right). \end{aligned} \tag{18}$$

The asthma-persistent equilibrium is given by

$$E^* = \left(N^*, A^*, L^*, B_1^*, B_2^*, B_3^*\right), \tag{19}$$

where

$$\begin{aligned} N^* &= \frac{\pi + \rho_1 B_1^*}{\beta + \eta + \alpha_1 + \delta_1},\ B_1^* = \frac{\alpha_1 N^*}{\rho_1 + \mu_1}, \\ A^* &= \frac{(\beta + \eta)N^* + wL^* + \rho_2 B_2^*}{r + r_1 + \alpha_2 + \delta_2},\ B_2^* = \frac{\alpha_2 A^*}{\rho_2 + \mu_2}, \\ L^* &= \frac{rA^* + r_1 B_1^* + \rho_3 B_3^*}{\alpha_3 + \delta_3 - w},\ B_3^* = \frac{\alpha_3 L^*}{\rho_3 + \mu_3 - \phi}. \end{aligned} \tag{20}$$

2.6 Reproductive Number

In order to find the reproductive number, we consider the system:

$$\begin{aligned} {}^C D_t^\theta B_1(t) &= \alpha_1 N - (\rho_1 + \mu_1)B_1, \\ {}^C D_t^\theta B_2(t) &= \alpha_2 A - (\rho_2 + \mu_2)B_2, \\ {}^C D_t^\theta B_3(t) &= \alpha_3 L + \phi B_3 - (\rho_3 + \mu_3)B_3. \end{aligned} \tag{21}$$

The matrices F and V^{-1} are calculated using the next generation matrix technique as follows:

$$F = \begin{bmatrix} \alpha_1 & 0 & 0 \\ 0 & \alpha_2 & 0 \\ 0 & 0 & \alpha_3 \end{bmatrix}, \; V^{-1} = \begin{bmatrix} \dfrac{1}{(\rho_1+\mu_1)} & 0 & 0 \\ 0 & \dfrac{1}{(\rho_2+\mu_2)} & 0 \\ 0 & 0 & \dfrac{1}{(\rho_3+\mu_3-\phi)} \end{bmatrix}. \tag{22}$$

Then, the reproduction number is obtained as

$$R_0 = max\left(\frac{\alpha_1}{(\rho_1+\mu_1)}, \frac{\alpha_2}{(\rho_2+\mu_2)}, \frac{\alpha_3}{(\rho_3+\mu_3-\phi)}\right). \tag{23}$$

2.7 Sensitivity of R_0

In the parameters model, the reproduction number R_0, which measures the disease distribution, has sensitivity indices that are found by sensitivity analysis. By calculating a parameter's uncertainty from its distribution, a frequency distribution for the fundamental reproduction number can be produced. It is possible to investigate the sensitivity of R_0 by taking into account important factors and computing partial derivatives of the reproductive number. Let

$$R_0^N = \frac{\alpha_1}{(\rho_1+\mu_1)}, \quad R_0^A = \frac{\alpha_2}{(\rho_2+\mu_2)}, \quad R_0^L = \frac{\alpha_3}{(\rho_3+\mu_3-\phi)}, \tag{24}$$

then, we calculate the sensitivity of R_0^N, R_0^A, and R_0^L as follows:

$$\frac{\partial R_0^N}{\partial \alpha_1} = \frac{1}{(\rho_1+\mu_1)} > 0, \; \frac{\partial R_0^N}{\partial \rho_1} = \frac{\partial R_0^N}{\partial \mu_1} = -\frac{\alpha_1}{(\rho_1+\mu_1)^2} < 0, \tag{25}$$

$$\frac{\partial R_0^A}{\partial \alpha_2} = \frac{1}{(\rho_2+\mu_2)} > 0, \; \frac{\partial R_0^A}{\partial \rho_2} = \frac{\partial R_0^A}{\partial \mu_2} = -\frac{\alpha_2}{(\rho_2+\mu_2)^2} < 0, \tag{26}$$

$$\frac{\partial R_0^L}{\partial \alpha_3} = \frac{1}{(\rho_3+\mu_3-\phi)} > 0, \; \frac{\partial R_0^L}{\partial \rho_3} = \frac{\partial R_0^L}{\partial \mu_3} = -\frac{\alpha_3}{(\rho_3+\mu_3-\phi)^2} < 0,$$

$$\frac{\partial R_0^L}{\partial \phi} = \frac{\alpha_3}{(\rho_3+\mu_3-\phi)^2} > 0. \tag{27}$$

An increase in that parameter's value will result in an increase in the related reproductive number since a positive value is directly proportional to related reproductive. Relative to related reproductive, a negative value is inversely proportional, meaning that if we raise the value of that parameter, the related reproductive number will fall. Sensitivity of these reproductive numbers with respect to these parameters is depicted in Figs. 2 and 3.

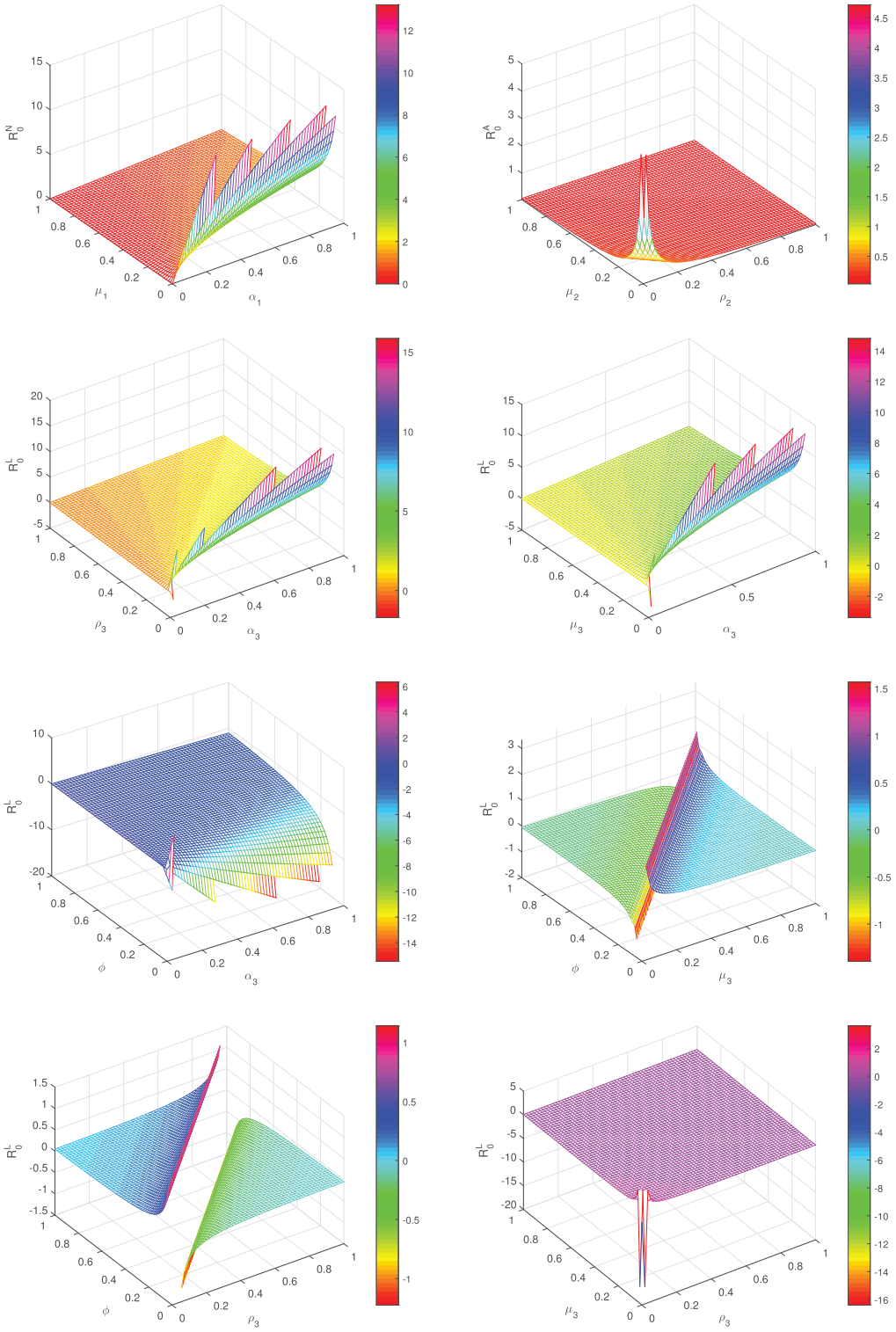

Figure 2: The sensitivity analysis of R_0's parameters

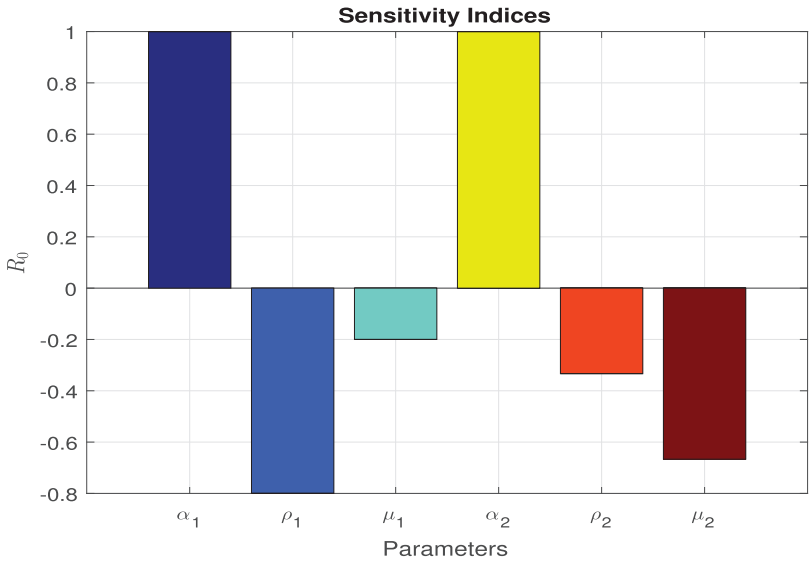

Figure 3: R_0's parameters Sensitivity Indices

3 Existence and Uniqueness Analysis

This study highlights the distinctiveness of the suggested Caputo model, which is founded on the Banach contraction principle and guarantees its existence and dependability in forecasting the dynamics of smoking-induced asthma. To enhance clarity and simplicity, we first assume the following four kernals:

$$\begin{aligned}
{}^{C}D^{\theta}_{0,t}N(t) &= \xi_1(t,N),\\
{}^{C}D^{\theta}_{0,t}A(t) &= \xi_2(t,A),\\
{}^{C}D^{\theta}_{0,t}L(t) &= \xi_3(t,L),\\
{}^{C}D^{\theta}_{0,t}B_1(t) &= \xi_4(t,B_1),\\
{}^{C}D^{\theta}_{0,t}B_2(t) &= \xi_5(t,B_2),\\
{}^{C}D^{\theta}_{0,t}B_3(t) &= \xi_6(t,B_3).
\end{aligned} \tag{28}$$

Applying the fractional-order Caputo operator to Eq. (16), we obtain

$$\begin{aligned}
N(t)-N(0) &= \varphi(\theta)\xi_1(t,N)+\psi(\theta)\int_0^t \xi_1(\chi,N)d\chi,\\
A(t)-A(0) &= \varphi(\theta)\xi_2(t,A)+\psi(\theta)\int_0^t \xi_2(\chi,A)d\chi,\\
L(t)-L(0) &= \varphi(\theta)\xi_3(t,L)+\psi(\theta)\int_0^t \xi_3(\chi,L)d\chi,\\
B_1(t)-B_1(0) &= \varphi(\theta)\xi_4(t,B_1)+\psi(\theta)\int_0^t \xi_4(\chi,B_1)d\chi,\\
B_2(t)-B_2(0) &= \varphi(\theta)\xi_5(t,B_2)+\psi(\theta)\int_0^t \xi_5(\chi,B_2)d\chi,\\
B_3(t)-B_3(0) &= \varphi(\theta)\xi_6(t,B_3)+\psi(\theta)\int_0^t \xi_6(\chi,B_3)d\chi,
\end{aligned} \tag{29}$$

where $\varphi(\theta)$ and $\psi(\theta)$ are the positive real constants. We will now establish the Lipschitz condition for the Caputo system (9).

Theorem 1. *The aforementioned kernals system* $\xi_1(t,N)$, $\xi_2(t,A)$, $\xi_3(t,L)$, $\xi_4(t,B_1)$, $\xi_5(t,B_2)$, *and* $\xi_6(t,B_3)$ *satisfy the Lipschitz condition.*

Proof. First, we justify the Lipschitz condition for the kernel ξ_1. Considering two function, N and $\hat{N}$, the corresponding norm is given by:

$$\begin{aligned} \| \xi_1(t,N) - \xi_1(t,\hat{N}) \| &\leq \| \left[\pi - (\beta+\eta)N - \alpha_1 N - \delta_1 N + \rho_1 B_1\right] - \left[\pi - (\beta+\eta)\hat{N} - \alpha_1\hat{N} - \delta_1\hat{N} + \rho_1\hat{B}_1\right] \|, \\ &\leq (\beta+\eta+\alpha_1+\delta_1) \| N - \hat{N} \| + \rho_1 \| B_1 - \hat{B}_1 \| . \end{aligned} \tag{30}$$

where β, η, α_1, δ_1, and ρ_1 are bounded functions. In the same way, the norms for the other model equations can be determined.

The subsequent recursive formula for (29) is the result of the Caputo model having at least one solution.

$$\begin{aligned} N_m(t) &= \varphi(\theta)\xi_1 + \psi(\theta)\int_0^t \xi_1(\chi, N_{m+1})d\chi, \\ A_m(t) &= \varphi(\theta)\xi_2 + \psi(\theta)\int_0^t \xi_2(\chi, A_{m+1})d\chi, \\ L_m(t) &= \varphi(\theta)\xi_3 + \psi(\theta)\int_0^t \xi_3(\chi, L_{m+1})d\chi, \\ B_{1m}(t) &= \varphi(\theta)\xi_4 + \psi(\theta)\int_0^t \xi_4(\chi, B_{1(m+1)})d\chi, \\ B_{2m}(t) &= \varphi(\theta)\xi_5 + \psi(\theta)\int_0^t \xi_5(\chi, B_{2(m+1)})d\chi, \\ B_{3m}(t) &= \varphi(\theta)\xi_6 + \psi(\theta)\int_0^t \xi_6(\chi, B_{3(m+1)})d\chi. \end{aligned} \tag{31}$$

The positive initial conditions are the first iterative values. Then

$$\begin{aligned} \Pi_{1m} &= N_m(t) - N_{m-1}(t), \\ &= \varphi(\theta)[\xi_1(t,N_{m-1}) - \xi_1(t,N_{m-2})] + \psi(\theta)\int_0^t [\xi_1(\chi,N_{m-1}) - \xi_1(\chi,N_{m-2})]d\chi, \end{aligned} \tag{32}$$

$$\begin{aligned} \Pi_{2m} &= A_m(t) - A_{m-1}(t), \\ &= \varphi(\theta)[\xi_2(t,A_{m-1}) - \xi_2(t,A_{m-2})] + \psi(\theta)\int_0^t [\xi_2(\chi,A_{m-1}) - \xi_2(\chi,A_{m-2})]d\chi, \end{aligned} \tag{33}$$

$$\begin{aligned} \Pi_{3m} &= L_m(t) - L_{m-1}(t), \\ &= \varphi(\theta)[\xi_3(t,L_{m-1}) - \xi_3(t,L_{m-2})] + \psi(\theta)\int_0^t [\xi_3(\chi,L_{m-1}) - \xi_3(\chi,L_{m-2})]d\chi, \end{aligned} \tag{34}$$

$$\begin{aligned} \Pi_{4m} &= B_{1(m)}(t) - B_{1(m-1)}(t), \\ &= \varphi(\theta)[\xi_4(t,B_{1(m-1)}) - \xi_4(t,B_{1(m-2)})] + \psi(\theta)\int_0^t [\xi_4(\chi,B_{1(m-1)}) - \xi_4(\chi,B_{1(m-2)})]d\chi, \end{aligned} \tag{35}$$

$$\begin{aligned} \Pi_{5m} &= B_{2(m)}(t) - B_{2(m-1)}(t), \\ &= \varphi(\theta)[\xi_5(t,B_{2(m-1)}) - \xi_5(t,B_{2(m-2)})] + \psi(\theta)\int_0^t [\xi_5(\chi,B_{2(m-1)}) - \xi_5(\chi,B_{2(m-2)})]d\chi, \end{aligned} \tag{36}$$

$$\begin{aligned}\Pi_{6m} &= B_{3(m)}(t) - B_{3(m-1)}(t),\\ &= \varphi(\theta)[\xi_6(t, B_{3(m-1)}) - \xi_6(t, B_{3(m-2)})] + \psi(\theta)\int_0^t [\xi_6(\chi, B_{3(m-1)}) - \xi_6(\chi, B_{3(m-2)})]d\chi.\end{aligned} \tag{37}$$

It is important to note that

$$\begin{aligned}&\sum_{j=0}^{m}\Pi_{1j} = N_m(t), \quad \sum_{j=0}^{m}\Pi_{2j} = A_m(t), \quad \sum_{j=0}^{m}\Pi_{3j} = L_m(t),\\ &\sum_{j=0}^{m}\Pi_{4j} = B_{1(m)}(t), \quad \sum_{j=0}^{m}\Pi_{5j} = B_{2(m)}(t), \quad \sum_{j=0}^{m}\Pi_{6j} = B_{3(m)}(t).\end{aligned} \tag{38}$$

Then, we have

$$\begin{aligned}\Pi_{1m} &= \| N_m(t) - N_{m-1}(t) \|,\\ &= \| \varphi(\theta)[\xi_1(t, N_{m-1}) - \xi_1(t, N_{m-2})] + \psi(\theta)\int_0^t [\xi_1(\chi, N_{m-1}) - \xi_1(\chi, N_{m-2})]d\chi \| .\end{aligned} \tag{39}$$

By applying the triangle inequality, the above equation can be reduced

$$\begin{aligned}\| N_m(t) - N_{m-1}(t) \| \le \varphi(\theta) \| [\xi_1(t, N_{m-1}) - \xi_1(t, N_{m-2})] \| + \psi(\theta) \| \int_0^t [\xi_1(\chi, N_{m-1})\\ - \xi_1(\chi, N_{m-2})]d\chi \| .\end{aligned} \tag{40}$$

Following from Eq. (29), the kernel $\xi_1(t, N)$ satisfies the Lipschitz condition. Consequently, it can be expressed as:

$$\| N_m(t) - N_{m-1}(t) \| \le \varphi(\theta)\zeta_1 \| N_{m-1} - N_{m-2} \| + \psi(\theta)\zeta_1 \int_0^t \| N_{m-1} - N_{m-2} \| d\chi. \tag{41}$$

We can simplify the above inequality as follows:

$$\| \Pi_{1m}(t) \| \le \varphi(\theta)\zeta_1 \| \Pi_{(m-1)}(t) \| + \psi(\theta)\zeta_1 \int_0^t \| \Pi_{(m-1)}(\chi) \| d\chi. \tag{42}$$

$$\| \Pi_{2m}(t) \| \le \varphi(\theta)\zeta_2 \| \Pi_{2(m-1)}(t) \| + \psi(\theta)\zeta_2 \int_0^t \| \Pi_{2(m-1)}(\chi) \| d\chi. \tag{43}$$

$$\| \Pi_{3m}(t) \| \le \varphi(\theta)\zeta_3 \| \Pi_{3(m-1)}(t) \| + \psi(\theta)\zeta_3 \int_0^t \| \Pi_{3(m-1)}(\chi) \| d\chi. \tag{44}$$

$$\| \Pi_{4m}(t) \| \le \varphi(\theta)\zeta_4 \| \Pi_{4(m-1)}(t) \| + \psi(\theta)\zeta_4 \int_0^t \| \Pi_{4(m-1)}(\chi) \| d\chi. \tag{45}$$

$$\| \Pi_{5m}(t) \| \le \varphi(\theta)\zeta_5 \| \Pi_{5(m-1)}(t) \| + \psi(\theta)\zeta_5 \int_0^t \| \Pi_{5(m-1)}(\chi) \| d\chi. \tag{46}$$

$$\| \Pi_{6m}(t) \| \le \varphi(\theta)\zeta_6 \| \Pi_{6(m-1)}(t) \| + \psi(\theta)\zeta_6 \int_0^t \| \Pi_{6(m-1)}(\chi) \| d\chi. \tag{47}$$

□

Theorem 2. *Given the condition:*

$$\varphi(\theta)\zeta_j + \psi(\theta)\zeta_j\Pi_{1,0} < 1, \quad j = 1, 2, ..., 6.$$

The fractional-order smoking-induces asthma system has an analytical solution at Π_0.

Proof. Following from the recursive relation, we observe that the all state variables are bounded functions, confirming that the Lipschitz criteria.

$$\| \Pi_{1m} \| \leq \| N(0) \| [\varphi(\theta)\zeta_j + \psi(\theta)\zeta_j t]^m \tag{48}$$

Although the solutions listed are legitimate, we take into consideration the following to make sure the functions listed accurately reflect the suggested model:

$$N(t) - N(0) = N_m(t) - \top_{1m}(t).$$

This implies that

$$\| \top_{1m}(t) \| \leq \| \varphi(\theta)[\xi_1(t, N_{m-1}) - \xi_1(t, N_{m-2})] + \psi(\theta) \int_0^t [\xi_1(\chi, N_{m-1}) - \xi_1(\chi, N_{m-2})] d\chi \| .$$

Using the Lipschitz condition,

$$\| \top_{1m}(t) \| \leq \varphi(\theta)\zeta_1 \| N - N_{m-1} \| + \psi(\theta)\zeta_1 \| N - N_{m-1} \| t. \tag{49}$$

This yields,

$$\| \top_{1m}(t) \| \leq [\varphi(\theta) + \psi(\theta)t]^{m+1}\zeta_1^{m+1}\varepsilon. \tag{50}$$

Next, at t_0, we obtain,

$$\| \top_{1m}(t) \| \leq [\varphi(\theta) + \psi(\theta)t_0]^{m+1}\zeta_1^{m+1}\varepsilon. \tag{51}$$

When m approaches ∞, we reach at

$$\| \top_{1m}(t) \| \to 0. \tag{52}$$

In the same direction, we may deduce

$$\begin{aligned} &\| \top_{2m}(t) \| \to 0, \\ &\| \top_{3m}(t) \| \to 0, \\ &\| \top_{4m}(t) \| \to 0, \\ &\| \top_{5m}(t) \| \to 0, \\ &\| \top_{6m}(t) \| \to 0. \end{aligned} \tag{53}$$

We must examine an other solution $N(t)$ to the suggested model in order to demonstrate the answer's uniqueness.

$$N(t) - \hat{N}(t) = \varphi(\theta)[\xi_1(t, N) - \xi_1(t, \hat{N})] + \psi(\theta) \int_0^t [\xi_1(\chi, N) - \xi_1(\chi, \hat{N})] d\chi. \tag{54}$$

Utilizing the norm in Eq. (54), we obtain

$$\| N(t) - \hat{N}(t) \| (1 - \varphi(\theta)\zeta_1 + \psi(\theta)\zeta_1 t) \leq 0. \tag{55}$$

□

Theorem 3. *In the following circumstance, the analytical solution for the Caputo fractional model is unique, which is:*

$$(1 - \varphi(\theta)\zeta_1 + \psi(\theta)\zeta_1 t) > 0. \tag{56}$$

Proof. Note that (56) is equivalent to (55) so that

$$\| N(t) - \hat{N}(t) \| (1 - \varphi(\theta)\zeta_1 + \psi(\theta)\zeta_1 t) \leq 0. \tag{57}$$

Thus,

$$\| N(t) - \hat{N}(t) \| = 0.$$

This suggests that the solution is distinctive and is therefore

$$N(t) = \hat{N}(t).$$

Also, we have

$$A(t) = \hat{A}(t), \quad L(t) = \hat{L}(t), \quad B_1(t) = \hat{B}_1(t), \quad B_2(t) = \hat{B}_2(t), \quad B_3(t) = \hat{B}_3(t). \tag{58}$$

□

4 Stability Analysis

Theorem 4. *The endemic equilibrium points E^* are globally asymptotically stable if the reproductive number mentioned in (23) is greater than 1.*

Proof. Let us represent the Lyapunov function:

$$F(N^*, A^*, L^*, B_1^*, B_2^*, B_3^*) \leq \left(N - N^* - N^* ln\frac{N^*}{N}\right) + \left(A - A^* - A^* ln\frac{A^*}{A}\right) + \left(L - L^* - L^* ln\frac{L^*}{L}\right) + \left(B_1 - B_1^* - B_1^* ln\frac{B_1^*}{B_1}\right) + \left(B_2 - B_2^* - B_2^* ln\frac{B_2^*}{B_2}\right) + \left(B_3 - B_3^* - B_3^* ln\frac{B_3^*}{B_3}\right). \tag{59}$$

Then, we have

$$\begin{aligned} {}^{C}D_t^{\theta} F \leq & \left(\frac{N - N^*}{N}\right) {}^{C}D_t^{\theta} N + \left(\frac{A - A^*}{A}\right) {}^{C}D_t^{\theta} A + \left(\frac{L - L^*}{L}\right) {}^{C}D_t^{\theta} L \\ & + \left(\frac{B_1 - B_1^*}{B_1}\right) {}^{C}D_t^{\theta} B_1 + \left(\frac{B_2 - B_2^*}{B_2}\right) {}^{C}D_t^{\theta} B_2 + \left(\frac{B_3 - B_3^*}{B_3}\right) {}^{C}D_t^{\theta} B_3. \end{aligned} \tag{60}$$

From (9), we can write as

$$
\begin{aligned}
{}^{C}D_t^{\theta}F \leq & \left(\frac{N-N^*}{N}\right)(\pi-(\beta+\eta)N-\alpha_1 N-\delta_1 N+\rho_1 B_1) \\
& +\left(\frac{A-A^*}{A}\right)((\beta+\eta)N+wL-(r+r_1)A-(\alpha_2+\delta_2)A+\rho_2 B_2) \\
& +\left(\frac{L-L^*}{L}\right)(rA+r_1 B_1-(\alpha_3+\delta_3-w)L+\rho_3 B_3)+\left(\frac{B_1-B_1^*}{B_1}\right)(\alpha_1 N-(\rho_1+\mu_1)B_1) \\
& +\left(\frac{B_2-B_2^*}{B_2}\right)(\alpha_2 A-(\rho_2+\mu_2)B_2)+\left(\frac{B_3-B_3^*}{B_3}\right)(\alpha_3 L+\phi B_3-(\rho_3+\mu_3)B_3)\,.
\end{aligned} \tag{61}
$$

Replacing $N = N - N^*$, $A = A - A^*$, $L = L - L^*$, $B_1 = B_1 - B_1^*$, $B_2 = B_2 - B_2^*$, $B_3 = B_3 - B_3^*$, we can have the following

$$
\begin{aligned}
{}^{C}D_t^{\theta}F \leq & \left(\frac{N-N^*}{N}\right)(\pi-(\beta+\eta)(N-N^*)-\alpha_1(N-N^*)-\delta_1(N-N^*)+\rho_1(B_1-B_1^*)) \\
& +\left(\frac{A-A^*}{A}\right)((\beta+\eta)(N-N^*)+w(L-L^*)-(r+r_1)(A-A^*)-(\alpha_2+\delta_2)(A-A^*)+\rho_2(B_2-B_2^*)) \\
& +\left(\frac{L-L^*}{L}\right)(r(A-A^*)+r_1(B_1-B_1^*)-(\alpha_3+\delta_3-w)(L-L^*)+\rho_3(B_3-B_3^*)) \\
& +\left(\frac{B_1-B_1^*}{B_1}\right)(\alpha_1(N-N^*)-(\rho_1+\mu_1)(B_1-B_1^*))+\left(\frac{B_2-B_2^*}{B_2}\right)(\alpha_2(A-A^*)-(\rho_2+\mu_2)(B_2-B_2^*)) \\
& +\left(\frac{B_3-B_3^*}{B_3}\right)(\alpha_3(L-L^*)+\phi(B_3-B_3^*)-(\rho_3+\mu_3)(B_3-B_3^*))\,.
\end{aligned} \tag{62}
$$

after some computations, we have

$${}^{C}D_t^{\theta}F \leq \Omega_1 - \Omega_2,$$

where

$$
\begin{aligned}
\Omega_1 = & \pi+\rho_1\beta_1\left(\frac{N-N^*}{N}\right)+(\beta+\eta)N\left(\frac{A-A^*}{A}\right)+wL\left(\frac{A-A^*}{A}\right)+\rho_2 B_2\left(\frac{A-A^*}{A}\right)+rA\left(\frac{L-L^*}{L}\right) \\
& +r_1 B_1\left(\frac{L-L^*}{L}\right)+\rho_3 B_3\left(\frac{L-L^*}{L}\right)+\alpha_1 N\left(\frac{B_1-B_1^*}{B_1}\right)+\alpha_2 A\left(\frac{B_2-B_2^*}{B_2}\right)+\alpha_3 L\left(\frac{B_3-B_3^*}{B_3}\right)+\phi\left(\frac{B_3-B_3^*}{B_3}\right).
\end{aligned} \tag{63}
$$

$$\Omega_2 = \pi\left(\frac{N^*}{N}\right) + (\beta+\eta)\left(\frac{(N-N^*)^2}{N}\right) + \alpha_1\left(\frac{(N-N^*)^2}{N}\right) + \delta_1\left(\frac{(N-N^*)^2}{N}\right) + \rho_1\beta_1^*\left(\frac{N-N^*}{N}\right)$$
$$+ (\beta+\eta)N^*\left(\frac{A-A^*}{A}\right) + wL^*\left(\frac{A-A^*}{A}\right) + (r+r_1)\left(\frac{(A-A^*)^2}{A}\right) + (\alpha_2+\delta_2)\left(\frac{(A-A^*)^2}{A}\right)$$
$$+ \rho_2 B_2^*\left(\frac{A-A^*}{A}\right) + rA^*\left(\frac{L-L^*}{L}\right) + r_1 B_1^*\left(\frac{L-L^*}{L}\right) + (\alpha_3+\delta_3-w)\left(\frac{(L-L^*)^2}{L}\right) + \rho_3 B_3^*\left(\frac{L-L^*}{L}\right)$$
$$+ \alpha_1 N^*\left(\frac{B_1-B_1^*}{B_1}\right) + (\rho_1+\mu_1)\left(\frac{(B_1-B_1^*)^2}{B_1}\right) + \alpha_2 A^*\left(\frac{B_2-B_2^*}{B_2}\right) + (\rho_2+\mu_2)\left(\frac{(B_2-B_2^*)^2}{B_2}\right)$$
$$+ \alpha_3 L^*\left(\frac{B_3-B_3^*}{B_3}\right) + (\rho_3+\mu_3)\left(\frac{(B_3-B_3^*)^2}{B_3}\right). \tag{64}$$

It follows that if $\lambda_1 < \lambda_2$, this results in ${}^{C}D_t^{\theta}L < 0$. However, when $N = N^*$, $A = A^*$, $L = L^*$, $B_1 = B_1^*$, $B_2 = B_2^*$, $B_3 = B_3^*$, we have

$$0 = \Omega_1 - \Omega_2 \quad \Rightarrow \quad {}^{C}D_t^{\theta}L = 0. \tag{65}$$

□

5 Chaos Control

Here, we discuss the use of linear feedback control method to stabilize system (9) at its equilibrium points, specifically focusing on the fractional-order system in its controlled form.

$$\begin{aligned}
{}^{C}D_t^{\theta}N(t) &= \pi - (\beta+\eta)N - \alpha_1 N - \delta_1 N + \rho_1 B_1 + \omega_1(N_t - N),\\
{}^{C}D_t^{\theta}A(t) &= (\beta+\eta)N + wL - (r+r_1)A - (\alpha_2+\delta_2)A + \rho_2 B_2 + \omega_2(A_t - A),\\
{}^{C}D_t^{\theta}L(t) &= rA + r_1 B_1 - (\alpha_3+\delta_3-w)L + \rho_3 B_3 + \omega_3(L_t - L),\\
{}^{C}D_t^{\theta}B_1(t) &= \alpha_1 N - (\rho_1+\mu_1)B_1 + \omega_4(B_{1t} - B_1),\\
{}^{C}D_t^{\theta}B_2(t) &= \alpha_2 A - (\rho_2+\mu_2)B_2 + \omega_5(B_{2t} - B_2),\\
{}^{C}D_t^{\theta}B_3(t) &= \alpha_3 L + \phi B_3 - (\rho_3+\mu_3)B_3 + \omega_6(B_{3t} - B_3),
\end{aligned} \tag{66}$$

where $\omega_1, \omega_2, \omega_3, \omega_4, \omega_5, \omega_6$ are control variables, therefore, the associated Jacobian matrix at is as follows:

$$J(E^{\circ}) = \begin{bmatrix}
-(\gamma_1+\omega_1) & 0 & 0 & \rho_1 & 0 & 0\\
(\beta+\eta) & -(\gamma_2+\omega_2) & w & 0 & \rho_2 & 0\\
0 & r & -(\gamma_3+\omega_3) & r_1 & 0 & \rho_3\\
\alpha_1 & 0 & 0 & -(\gamma_4+\omega_4) & 0 & 0\\
0 & \alpha_2 & 0 & 0 & -(\gamma_5+\omega_5) & 0\\
0 & 0 & \alpha_3 & 0 & 0 & -(\gamma_6+\omega_6+\phi)
\end{bmatrix}, \tag{67}$$

where

$$\begin{aligned}
\gamma_1 &= \beta + \eta + \alpha_1 + \delta_1,\\
\gamma_2 &= r + r_1 + \alpha_2 + \delta_2,\\
\gamma_3 &= \alpha_3 + \delta_3 - w,\\
\gamma_4 &= \rho_1 + \mu_1,\\
\gamma_5 &= \rho_2 + \mu_2,\\
\gamma_6 &= \rho_3 + \mu_3.
\end{aligned} \tag{68}$$

With the chosen values $\omega_1 = 1$, $\omega_2 = 2$, $\omega_3 = 3$, $\omega_4 = 4$, $\omega_5 = 5$, $\omega_6 = 6$, the characteristic polynomial is given by:

$$Z(\lambda) = \begin{bmatrix}
\lambda + \gamma_1 + \omega_1 & 0 & 0 & -\rho_1 & 0 & 0\\
-\beta - \eta & \lambda + \gamma_2 + \omega_2 & -w & 0 & -\rho_2 & 0\\
0 & -r & \lambda + \gamma_3 + \omega_3 & -r_1 & 0 & -\rho_3\\
-\alpha_1 & 0 & 0 & \lambda + \gamma_4 + \omega_4 & 0 & 0\\
0 & -\alpha_2 & 0 & 0 & \lambda + \gamma_5 + \omega_5 & 0\\
0 & 0 & -\alpha_3 & 0 & 0 & \lambda + \gamma_6 + \omega_6 + \phi
\end{bmatrix}. \tag{69}$$

Furthermore, the computed characteristic roots are:

$$\lambda_1 = -1.2687, \quad \lambda_2 = -1.2106, \quad \lambda_3 = -0.5911, \quad \lambda_4 = -0.3207, \quad \lambda_5 = -0.2593, \quad \lambda_6 = -0.279.$$

Since all eigenvalues have negative real parts, the equilibrium point E_0 is asymptotically stable. Figs. 4–8 show the chaos control of the proposed model for all groups.

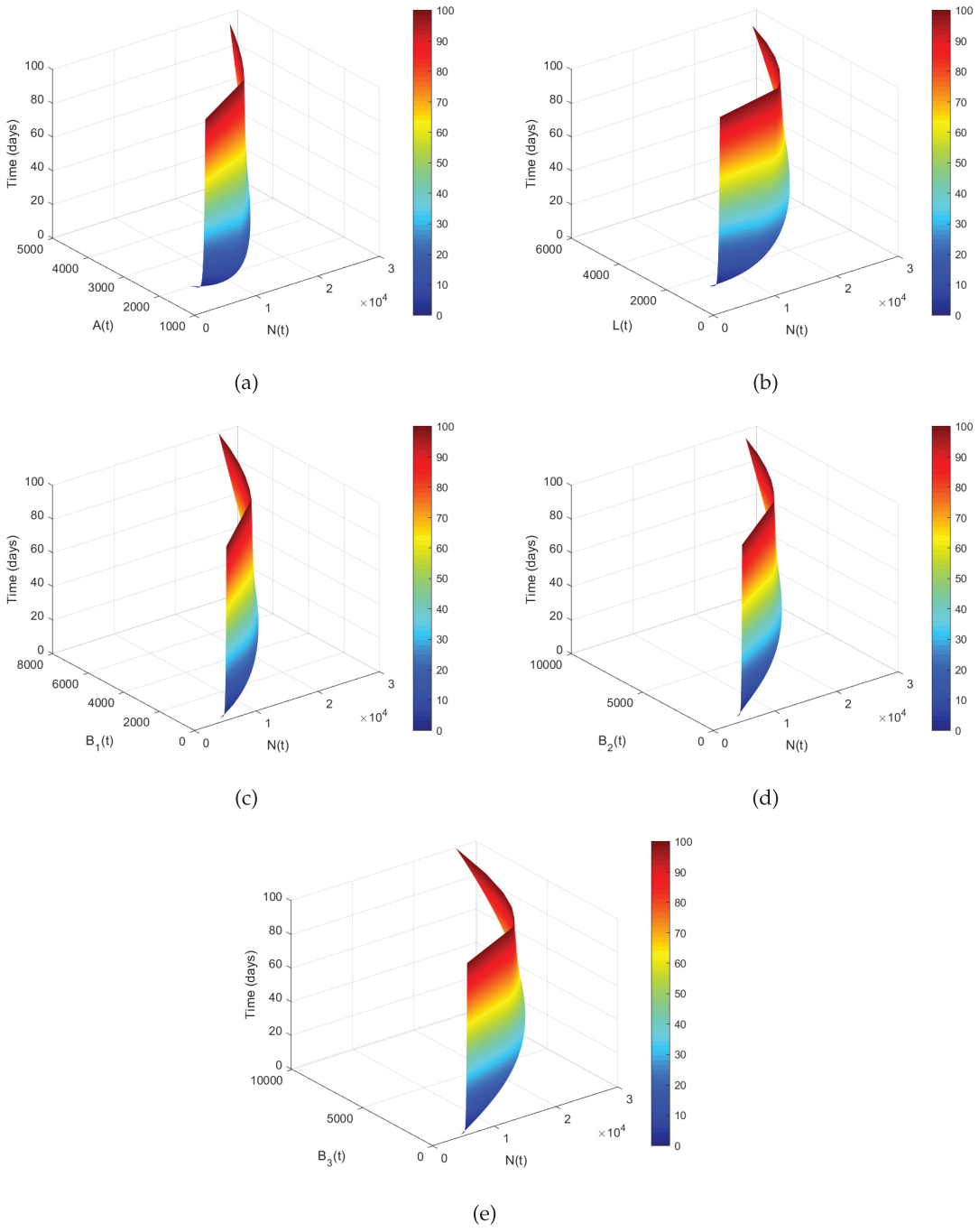

Figure 4: Co-relation between $N(t)$ with other compartments

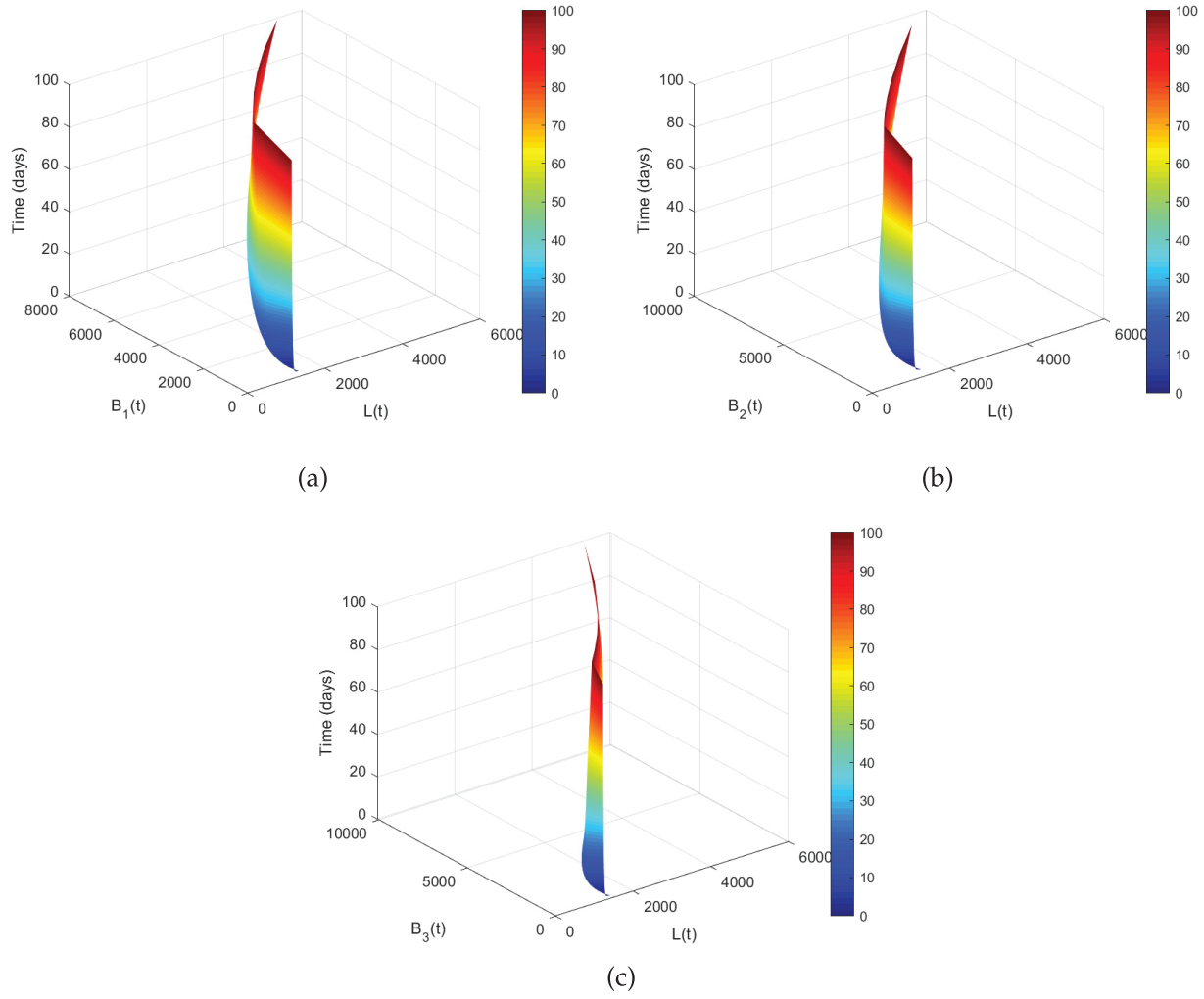

Figure 5: Co-relation between $L(t)$ with other compartments

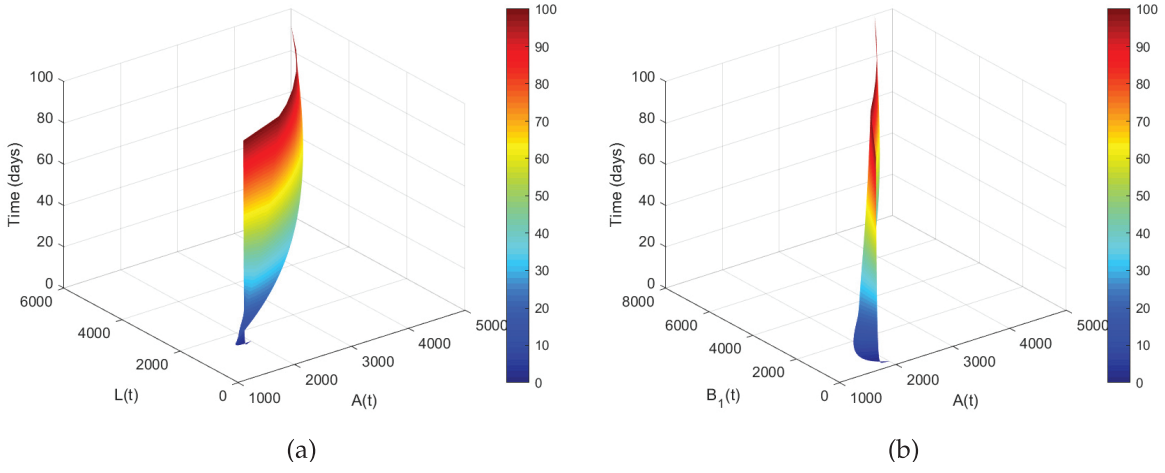

Figure 6: (Continued)

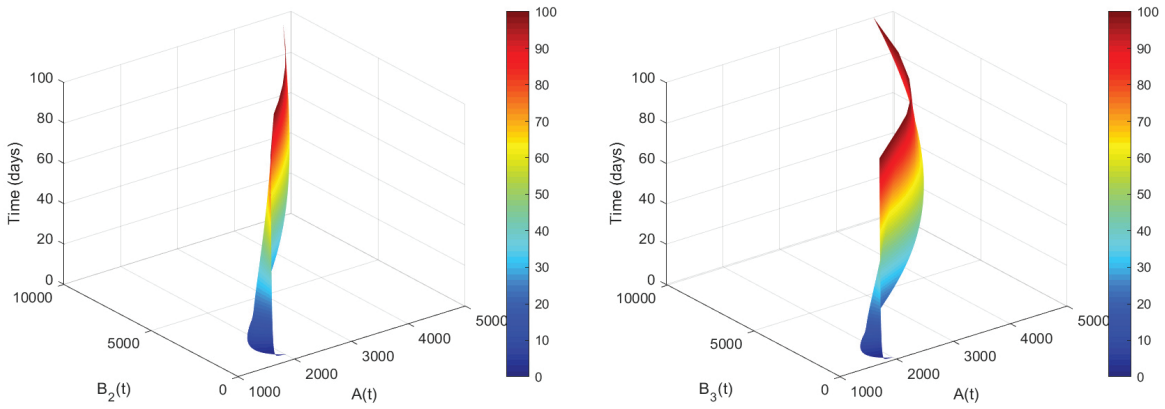

Figure 6: Co-relation between $A(t)$ with other compartments

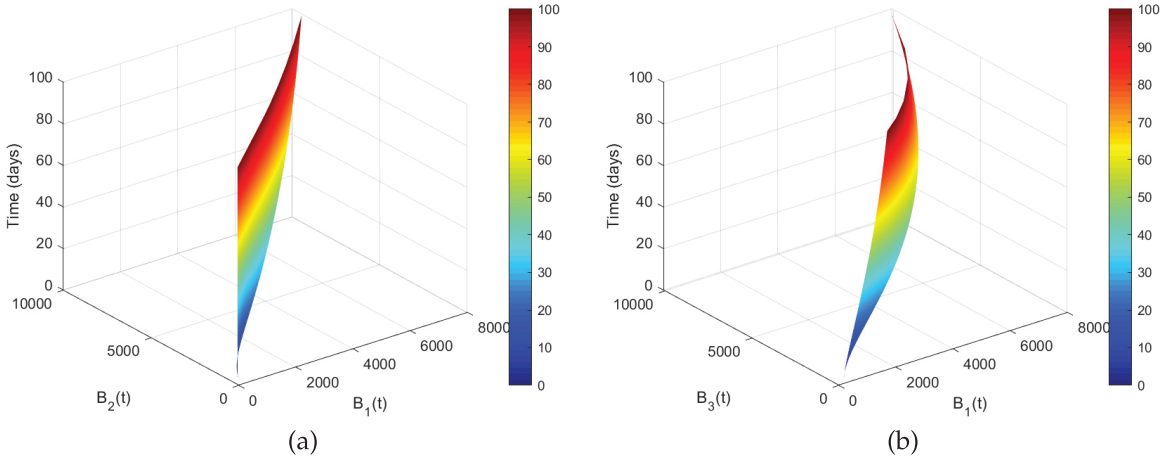

Figure 7: Co-relation between $B_1(t)$ with other compartments

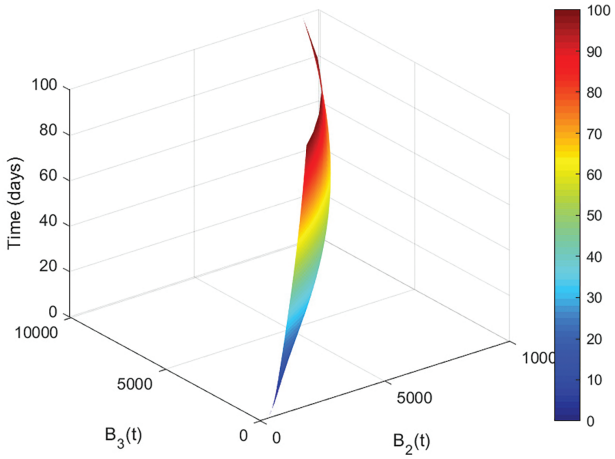

Figure 8: Co-relation between $B_2(t)$ with other compartments

Fig. 4 displays a set of graphs that show the co-relation between $N(t)$ and other compartments. A smooth 3D surface is shown by the first Fig. 4a, where $N(t)$ falls as $A(t)$ rises. This implies that the number of people with asthma increases over time as the number of non-smokers declines. This finding implies that exposure to smoking by non-smokers may be a factor in the rise in asthmatic people. A 3D surface plot with $L(t)$ growing initially as $N(t)$ lowers is shown in Fig. 4b. Thus, smoking exposure raises the latent population before the disease manifests itself. The 3D surface plot in Fig. 4c demonstrates a steady increase in $B_1(t)$ as $N(t)$ decreases. Since fewer healthy non-smokers translate into more bronchial problems, the slope indicates a strong negative correlation. In Fig. 4d, $B_2(t)$ increases when $N(t)$ decreases, much like in Fig. 4c. Compared to $B_1(t)$, the growth is more gradual, indicating a slower migration into the $B_2(t)$ class. Some non-smokers develop asthma quickly, while others gradually develop impaired bronchial function. As $N(t)$ falls, the Fig. 4e displays the greatest increase in $B_3(t)$. The curve shows that serious difficulties rise quickly as more non-smokers leave their class. Fig. 4 demonstrates that asthmatic-related compartments $(A(t), L(t), B_1(t), B_2(t), and\, B_3(t))$ rise in proportion to the decrease in non-smokers $N(t)$.

The co-relation between the exposed class $L(t)$ and other model compartments is depicted in Fig. 5. As $L(t)$ rises in Fig. 5a, $B_1(t)$ also climbs gradually over time. People who are more exposed are more likely to get respiratory issues. In contrast to $B_1(t)$, Fig. 5b exhibits a similar pattern more slowly. As $L(t)$ declines at later points in Fig. 5c, $B_3(t)$ rises rapidly. Long-term exposure eventually speeds up the development of serious asthmatic problems. Exposure is a crucial intermediary step that connects non-smokers to the whole course of asthma in Fig. 5.

The interactions between the asthmatic class and other disease-related groups are depicted in Fig. 6. In Fig. 6a, the exposed class initially maintains expansion as the number of asthmatic individuals rises. More bronchial respiratory damage results from a larger prevalence of asthma, as shown in Fig. 6b. The gradual but steady increase of $B_2(t)$ with $A(t)$ is shown in Fig. 6c. The deadly endpoint of smoking-induced asthma is highlighted by the progression of uncontrolled asthma into severe bronchial problems (Fig. 6d). Thus, asthma is the primary cause of disease progression.

The interaction between the population with initial asthma and other illness states throughout time is depicted in Fig. 7. There is a strong positive association shown in Fig. 7a; as $B_1(t)$ climbs over time, so does $B_2(t)$. Asthma is a sign of deteriorating bronchial function, which is a result of smoking-induced disease progression. Similarly, Fig. 7b shows a straight positive relationship between $B_1(t)$ and the severe asthma class $B_3(t)$. Accordingly, the asthma class $B_1(t)$ serves as a transitional condition, emphasizing its function as an early indicator of deteriorating illness.

The intermediate stage, where asthma functions are compromised, is the subject of Fig. 8. There is a definite monotonic increase: $B_3(t)$ climbs gradually as $B_2(t)$ rises. Severe asthma is represented by $B_2(t)$, which is a transitional state that feeds into $B_3(t)$. As a result, the system smoothly approaches equilibrium states.

6 Numerical Scheme

To approximate the Caputo fractional system, we employ the Newton-polynomial based scheme for the proposed model (9) originally introduced by [30]. To simplify the explanation, we can represent the previously mentioned system as follows:

$$
\begin{aligned}
{}^{C}D_t^{\theta} N(t) &= \varpi_1(t, N),\\
{}^{C}D_t^{\theta} A(t) &= \varpi_2(t, A),\\
{}^{C}D_t^{\theta} L(t) &= \varpi_3(t, L),
\end{aligned}
$$

$$
\begin{aligned}
{}^{C}D_t^{\theta}B_1(t) &= \varpi_4(t, B_1),\\
{}^{C}D_t^{\theta}B_2(t) &= \varpi_5(t, B_2),\\
{}^{C}D_t^{\theta}B_3(t) &= \varpi_6(t, B_3).
\end{aligned} \tag{70}
$$

At $t_{j+1} = (j+1)\Delta t$, we have the following:

$$
N(t_{j+1}) = N(0) + \frac{1-\theta}{\Gamma(\theta)}\sum_{d=2}^{j}\int_{t_d}^{t_{d+1}} \varpi_1(\tau, N(\tau))(t_{j+1}-\tau)^{\theta-1}d\tau. \tag{71}
$$

Above equation can be modified by using the Newton polynomial as

$$
\begin{aligned}
N^{j+1} &= N_0 + \frac{1-\theta}{\Gamma(\theta)}\sum_{d=2}^{j}\int_{t_d}^{t_{d+1}} \varpi_1(t_{d-2}, N^{d-2}) + \frac{\varpi_1(t_{d-1}, N^{d-1}) - \varpi_1(t_{d-2}, N^{d-2})}{\Delta t}(\tau, t_{d-2})\\
&\quad + \frac{\varpi_1(t_d, N^d) - 2\varpi_1(t_{d-1}, N^{d-1}) + \varpi_1(t_{d-2}, N^{d-2})}{2(\Delta t)^2}(\tau - t_{d-2})(\tau - t_{d-1})[(t_{j+1}-\tau)^{\theta-1}]d\tau.
\end{aligned} \tag{72}
$$

We get finally the following:

$$
\begin{aligned}
N^{j+1} &= N_0 + \frac{(\Delta t)^{\theta}}{\Gamma(\theta+1)}\sum_{d=2}^{j}\varpi_1(t_{d-2}, N^{d-2})\hbar + \frac{(\Delta t)^{\theta}}{\Gamma(\theta+2)}\sum_{d=2}^{j}[\varpi_1(t_{d-1}, N^{d-1}) - \varpi_1(t_{d-2}, N^{d-2})]\hbar_1\\
&\quad + \frac{(\Delta t)^{\theta}}{2\Gamma(\theta+3)}\sum_{d=2}^{j}[\varpi_1(t_d, N^d) - 2\varpi_1(t_{d-1}, N^{d-1}) + \varpi_1(t_{d-2}, N^{d-2})]\hbar_2.
\end{aligned} \tag{73}
$$

$$
\begin{aligned}
A^{j+1} &= A_0 + \frac{(\Delta t)^{\theta}}{\Gamma(\theta+1)}\sum_{d=2}^{j}\varpi_2(t_{d-2}, N^{d-2})\hbar + \frac{(\Delta t)^{\theta}}{\Gamma(\theta+2)}\sum_{d=2}^{j}[\varpi_2(t_{d-1}, N^{d-1}) - \varpi_2(t_{d-2}, N^{d-2})]\hbar_1\\
&\quad + \frac{(\Delta t)^{\theta}}{2\Gamma(\theta+3)}\sum_{d=2}^{j}[\varpi_2(t_d, N^d) - 2\varpi_2(t_{d-1}, N^{d-1}) + \varpi_2(t_{d-2}, N^{d-2})]\hbar_2.
\end{aligned} \tag{74}
$$

$$
\begin{aligned}
L^{j+1} &= L_0 + \frac{(\Delta t)^{\theta}}{\Gamma(\theta+1)}\sum_{d=2}^{j}\varpi_3(t_{d-2}, N^{d-2})\hbar + \frac{(\Delta t)^{\theta}}{\Gamma(\theta+2)}\sum_{d=2}^{j}[\varpi_3(t_{d-1}, N^{d-1}) - \varpi_3(t_{d-2}, N^{d-2})]\hbar_1\\
&\quad + \frac{(\Delta t)^{\theta}}{2\Gamma(\theta+3)}\sum_{d=2}^{j}[\varpi_3(t_d, N^d) - 2\varpi_3(t_{d-1}, N^{d-1}) + \varpi_3(t_{d-2}, N^{d-2})]\hbar_2.
\end{aligned} \tag{75}
$$

$$
\begin{aligned}
B_1^{j+1} &= B_{10} + \frac{(\Delta t)^{\theta}}{\Gamma(\theta+1)}\sum_{d=2}^{j}\varpi_4(t_{d-2}, N^{d-2})\hbar + \frac{(\Delta t)^{\theta}}{\Gamma(\theta+2)}\sum_{d=2}^{j}[\varpi_4(t_{d-1}, N^{d-1}) - \varpi_4(t_{d-2}, N^{d-2})]\hbar_1\\
&\quad + \frac{(\Delta t)^{\theta}}{2\Gamma(\theta+3)}\sum_{d=2}^{j}[\varpi_4(t_d, N^d) - 2\varpi_4(t_{d-1}, N^{d-1}) + \varpi_4(t_{d-2}, N^{d-2})]\hbar_2.
\end{aligned} \tag{76}
$$

$$B_2^{j+1} = B_{20} + \frac{(\Delta t)^\theta}{\Gamma(\theta+1)} \sum_{d=2}^{j} \varpi_5(t_{d-2}, N^{d-2})\hbar + \frac{(\Delta t)^\theta}{\Gamma(\theta+2)} \sum_{d=2}^{j} [\varpi_5(t_{d-1}, N^{d-1}) - \varpi_5(t_{d-2}, N^{d-2})]\hbar_1$$
$$+ \frac{(\Delta t)^\theta}{2\Gamma(\theta+3)} \sum_{d=2}^{j} [\varpi_5(t_d, N^d) - 2\varpi_5(t_{d-1}, N^{d-1}) + \varpi_5(t_{d-2}, N^{d-2})]\hbar_2. \quad (77)$$

$$B_3^{j+1} = B_{30} + \frac{(\Delta t)^\theta}{\Gamma(\theta+1)} \sum_{d=2}^{j} \varpi_6(t_{d-2}, N^{d-2})\hbar + \frac{(\Delta t)^\theta}{\Gamma(\theta+2)} \sum_{d=2}^{j} [\varpi_6(t_{d-1}, N^{d-1}) - \varpi_6(t_{d-2}, N^{d-2})]\hbar_1$$
$$+ \frac{(\Delta t)^\theta}{2\Gamma(\theta+3)} \sum_{d=2}^{j} [\varpi_6(t_d, N^d) - 2\varpi_6(t_{d-1}, N^{d-1}) + \varpi_6(t_{d-2}, N^{d-2})]\hbar_2. \quad (78)$$

$$\hbar = [(j-d+1)^\theta - (j-b)^\theta],$$
$$\hbar_1 = [(j-d+1)^\theta(j-d+3+2\theta) - (j-b)^\theta(j-d+3+3\theta)],$$
$$\hbar_2 = [(j-d+1)^\theta[2(j-d)^2 + (3\theta+10)(j-d) + 2\theta^2 + 9\theta + 12].$$

7 Numerical Simulation

The proposed dynamical model (9) depicts the interplay between smoking and asthma as a nonlinear dynamical system. This section of the article presents the results and analysis for the analytical solution of the suggested fractional equations. After a small number of repetitions, it is believed that the predicted results, as stated in the section above, quickly approach the precise solution. We used MATLAB for numerical simulations by choosing appropriate initial conditions and parameter values. These values are suggested on the previous works done in [33–35]. The parameters values used in numerical simulations are as follows: $\pi = 1000$; $\beta = 0.02$; $\eta = 0.005$; $\alpha_1 = 0.01$; $\rho_1 = 0.02$; $\delta_1 = 0.005$; $w = 0.01$; $r = 0.03$; $r_1 = 0.05$; $\alpha_2 = 0.08$; $\rho_2 = 0.01$; $\delta_2 = 0.01$; $\alpha_3 = 0.05$; $\rho_3 = 0.015$; $\delta_3 = 0.07$; $\phi = 0.02$; $\mu_1 = 0.005$; $\mu_2 = 0.02$; and $\mu_1 = 0.01$. Systems with long-term dependencies or memory are frequently described using fractional calculus. Because of this, we experimented with several fractional order θ values and compared the outcomes with the integer-order situation.

The set of graphs presented in Fig. 9 illustrates the behavior of $N(t)$ over time under different fractional orders scenarios. The first Fig. 9a provides a comparison of $N(t)$ under integer and fractional orders. It is evident that for integer-order models ($\theta = 1$), $N(t)$ exhibits the fastest growth rate, reaching higher values within a shorter time. As the fractional order decreases, the progression of $N(t)$ slows down, highlighting the effect of memory and hereditary properties in the system. This observation suggests that fractional-order derivatives introduce a delay in the response of $N(t)$, which can be crucial in modeling real-world biological systems. Fig. 9b presents a 3D surface plot of $N(t)$, illustrating its evolution over time and different fractional orders. The peak of the surface represents the maximum value attained by $N(t)$, while the gradual increase and decline showcase how different fractional orders influence its trajectory. To demonstrate the system's continuous response, Fig. 9c examines the surface's smooth transitions. Figures show that $N(t)$ rises with increasing fractional order, whereas lesser orders climb more gradually. Therefore, fractional calculus is perfect for real-world applications since it can regulate the behavior of systems. As a contour diagram, the plot (Fig. 9d) shows the distribution of the $N(t)$ variable over time t against the θ values. Darker regions provide lower θ values, while lighter regions help to highlight higher θ values. The variations in contours further support the finding that fractional derivatives influence the degree at which $N(t)$ evolves, indicating the value of fractional-order models in describing the dynamics of intricate structures. The overall findings attest to the importance of fractional calculus in improving the mathematical description of $N(t)$.

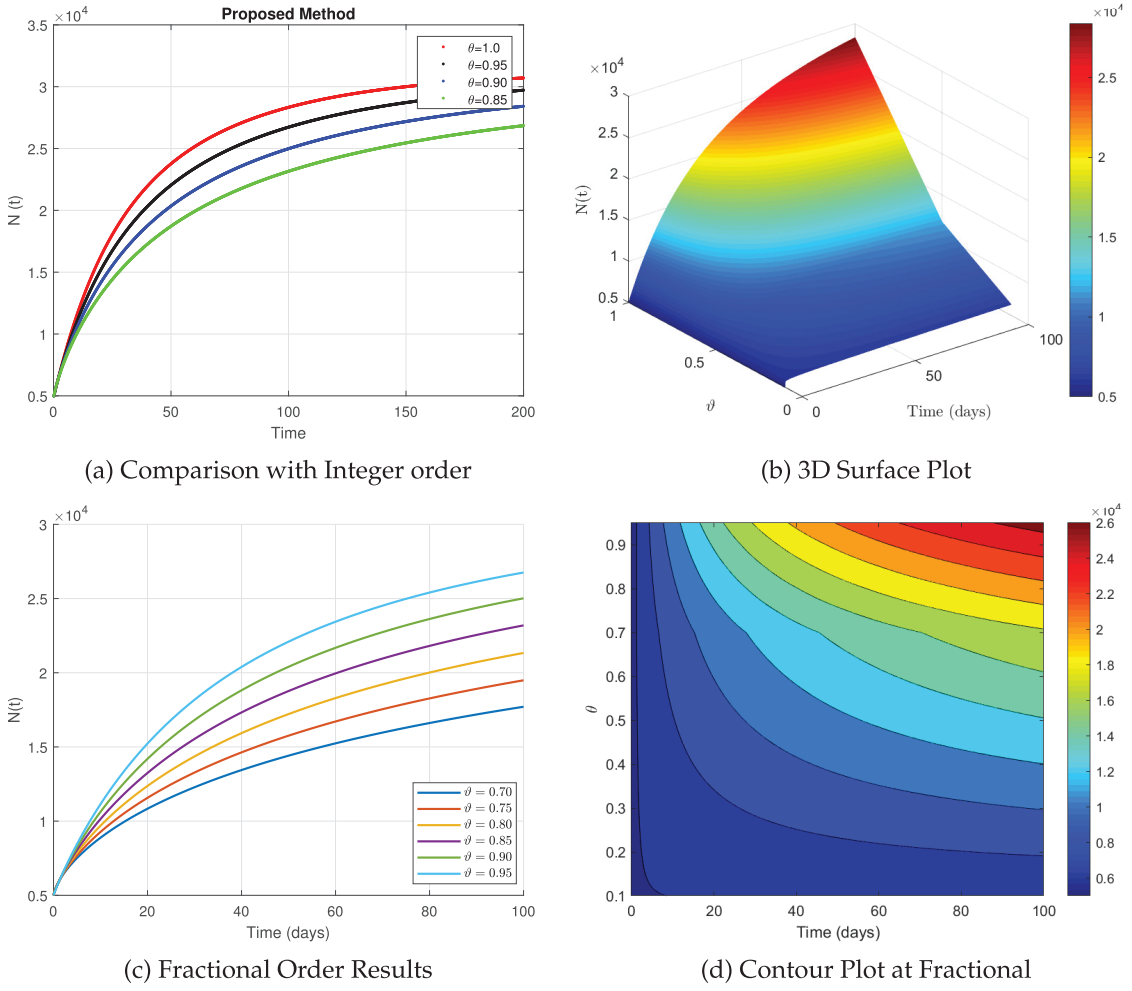

(a) Comparison with Integer order

(b) 3D Surface Plot

(c) Fractional Order Results

(d) Contour Plot at Fractional

Figure 9: The simulation of $N(t)$ at different fractional order

Fig. 10, in Fig. 10a the integer-order model ($\theta = 1$), shows a more rapid increase in affected individuals. As the fractional order decreases, the growth slows down, indicating that memory effects delay the progression of asthma cases. Fig. 10b shows the evolution of asthma cases over time. A peak appears, signifying the maximum number of cases before a possible stabilization. In Fig. 10c, different fractional values affect the rate of disease spread. Lower fractional orders ($\theta < 1$) slow down the increase in cases. Fig. 10d visualizes how different fractional orders influence the number of asthma cases. Lighter areas indicate a higher number of affected individuals over time.

In Fig. 11a, the integer-order model shows a fast progression of lung damage cases. Fractional models demonstrate a slower onset due to memory effects. Fig. 11b depicts the gradual accumulation of lung damage over time. The peak suggests that lung damage worsens before stabilizing. In Fig. 11c, a higher fractional order leads to a more rapid increase in lung damage. Lower orders indicate a slower progression, which aligns with real-world cases where damage accumulates gradually. Fig. 11d represents different intensity levels of lung damage. The color variations highlight how the disease progresses under different fractional orders. These results highlight the importance of fractional calculus in modeling asthma and lung damage, capturing real-world memory effects and delayed responses in disease progression.

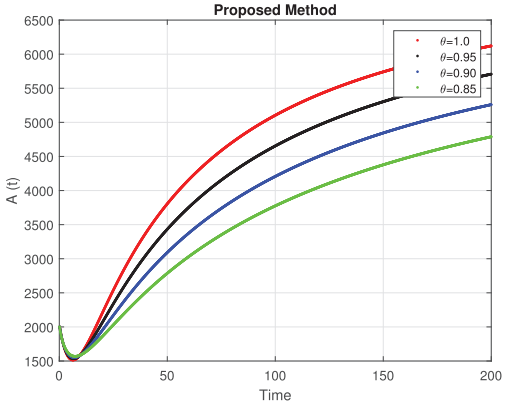

(a) Comparison with Integer order

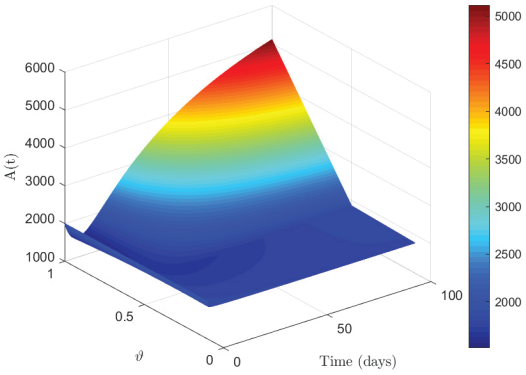

(b) 3D Surface Plot

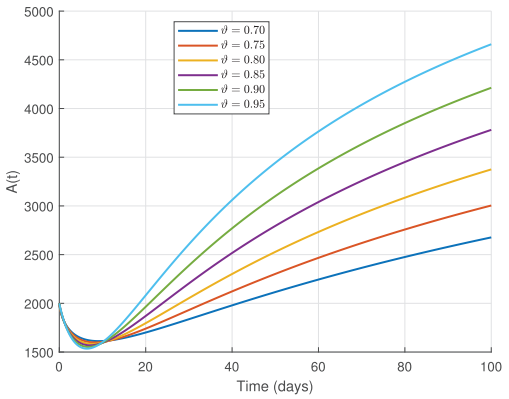

(c) Fractional Order Results

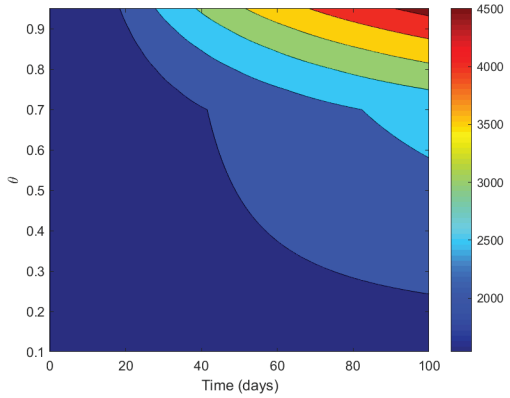

(d) Contour Plot at Fractional

Figure 10: The simulation of $A(t)$ at different fractional order

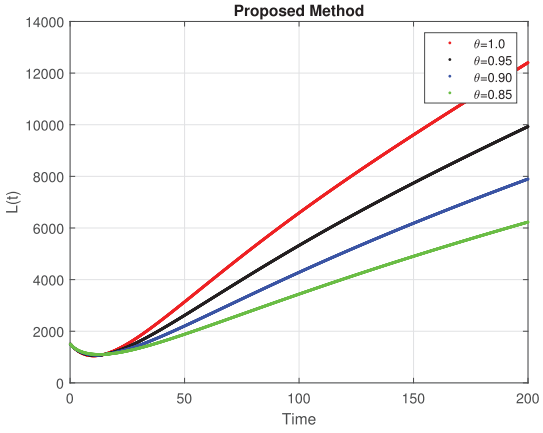

(a) Comparison with Integer order

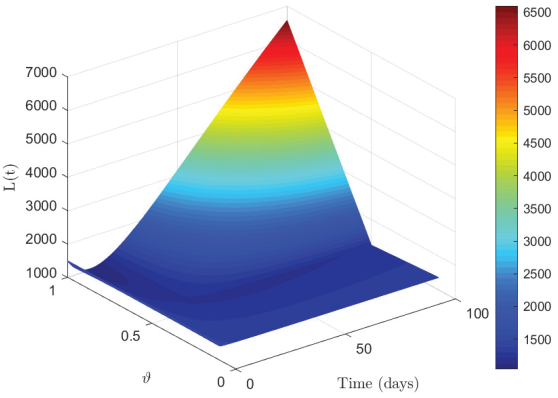

(b) 3D Surface Plot

Figure 11: (Continued)

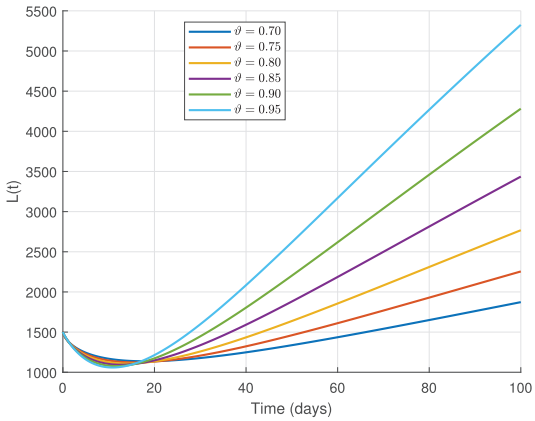

(c) Fractional Order Results

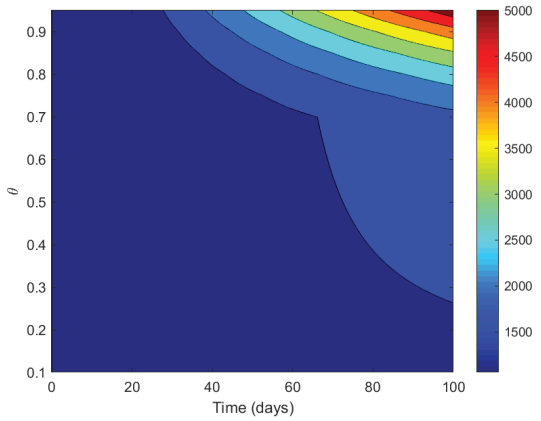

(d) Contour Plot at Fractional

Figure 11: The simulation of $L(t)$ at different fractional order

Fig. 12a, the integer-order model ($\theta = 1$), shows the fastest increase in $B_1(t)$. As the fractional order decreases, the growth slows down, indicating a delay in disease progression due to memory effects. Fig. 12b illustrates how $B_1(t)$ evolves over time. The peak suggests a point where disease progression reaches its highest before stabilizing. Fig. 12c shows the impact of different fractional orders. Smaller orders indicate a delayed response, while larger values indicate quick progression. The dispersion of $B_1(t)$ against time is shown in Fig. 12d. Larger values for $B_1(t)$ are indicated by light patches, while slow progression is indicated by dark parts. The graphic illustrates how memory effects impact progression and how fractional operators affect disease dynamics.

Fig. 13 provides a detailed description of the simulated dynamics of $B_2(t)$. According to the Fig. 13a, the integer-order model grew at the quickest rate during the time period, with $B_2(t)$ showing a slow climb at lower fractional orders. This demonstrates that fractional order (θ) modeling has greater dynamics when it comes to observing the behavior of complex systems. In contrast to the top surface, which takes large values of $B_2(t)$ and increases extremely quickly within specific measurements, the lower surface fluctuates less, according to the 3D surface plot shown in Fig. 13b. The surface slope of the suggested system emphasizes a more gradual transition in system performance. Additionally, as shown in Fig. 13c, the system response significantly alters with changes in fractional order. We find that greater θ values develop significantly faster than lower fractional orders, which take longer to grow. The time-and-fractional-order distribution of $B_2(t)$ is specifically displayed in a contour plot, as seen in Fig. 13d. This explains exactly how B(t) growth processes are modified by fractional operators. This demonstrates the usefulness of the fractional-order (θ) in understanding complex models.

Fig. 14a shows the dynamics of the $B_3(t)$ class at various fractional orders. The system's evolution demonstrates the effectiveness of Caputo derivative. The memory effects are demonstrated by the non-local fractional derivative, which slows down the time dependence of $B_3(t)$. The increase is slower in the fractional-order situation than in the integer-order case. The 3D surface plot in Fig. 14b illustrates this. In contrast to the integer-order models, the results of the fractional-order θ behavior modeling of the suggested system are extremely accurate and smooth. Fig. 14c shows the transmission dynamics of $B_3(t)$ at different θ values. We find that slower growth rates are indicated by smaller θ values. This guarantees the Caputo fractional derivative's flexibility in controlling the evolution of the suggested system and,

consequently, characterizing complicated systems. The contour map in Fig. 14d is created by varying θ values, demonstrating the amount of fractional calculus required to explain dynamic variations in $B_3(t)$.

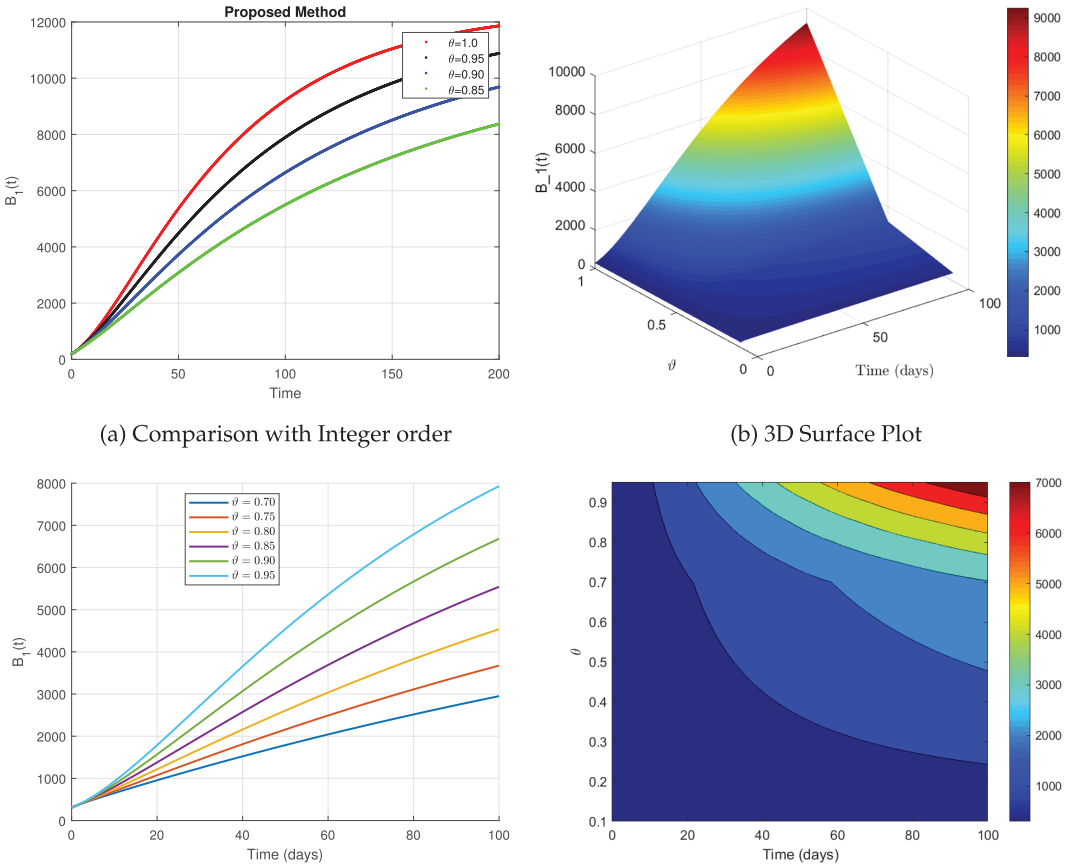

(a) Comparison with Integer order

(b) 3D Surface Plot

(c) Fractional Order Results

(d) Contour Plot at Fractional

Figure 12: The simulation of $B_1(t)$ at different fractional order

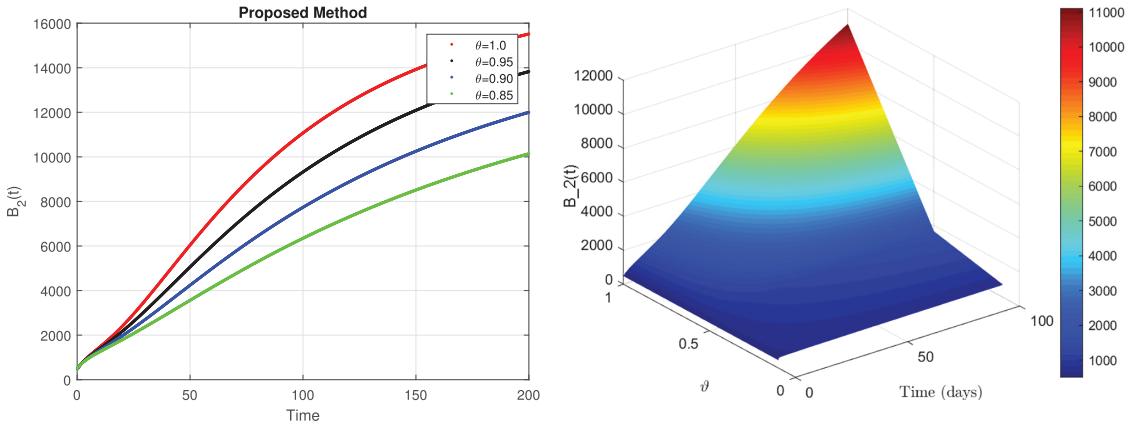

(a) Comparison with Integer order

(b) 3D Surface Plot

Figure 13: (Continued)

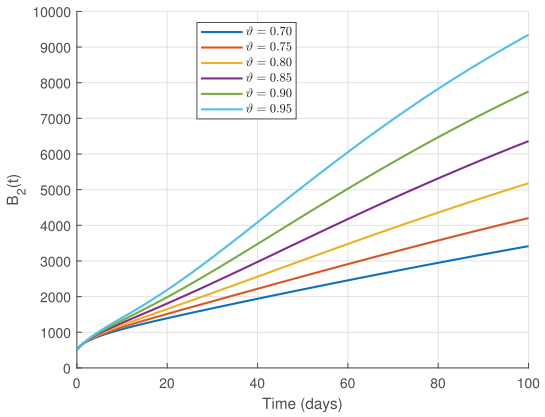

(c) Fractional Order Results

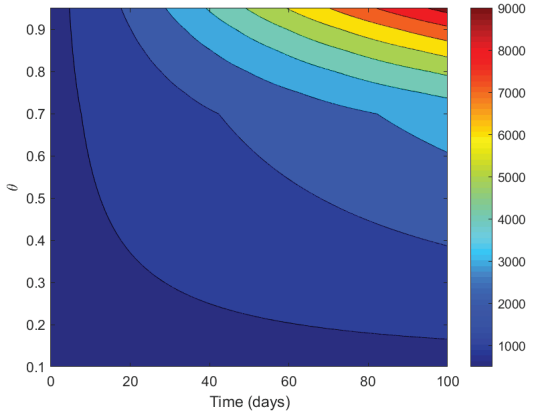

(d) Contour Plot at Fractional

Figure 13: The simulation of $B_2(t)$ at different fractional order

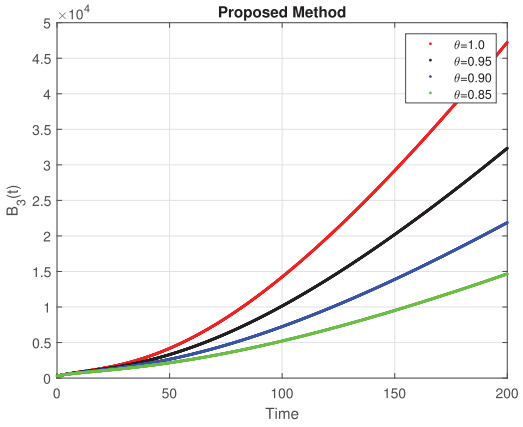

(a) Comparison with Integer order

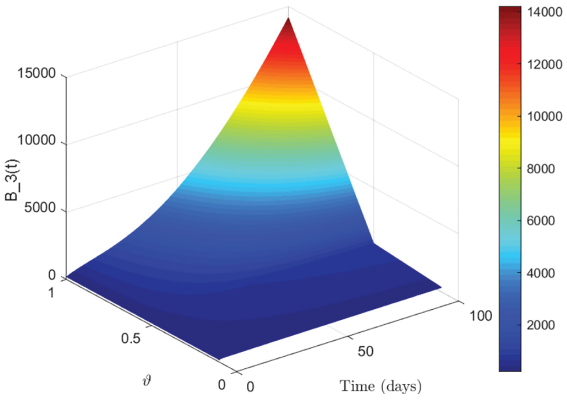

(b) 3D Surface Plot

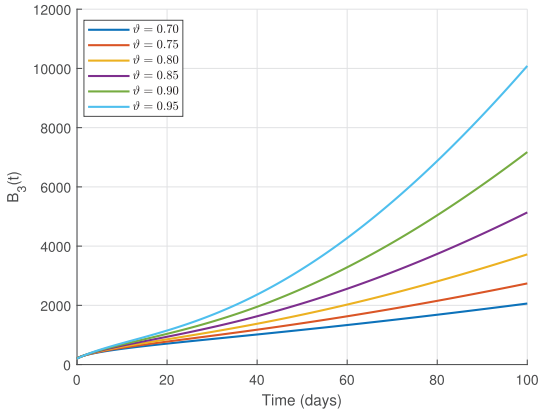

(c) Fractional Order Results

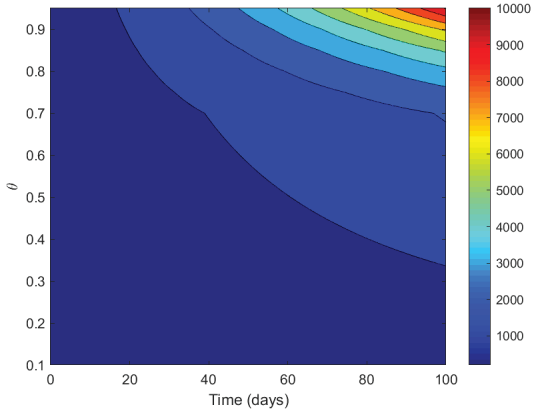

(d) Contour Plot at Fractional

Figure 14: The simulation of $B_3(t)$ at different fractional order

8 Conclusion

This study used a fractional-order mathematical model to examine how smoking affects the development of asthma. To establish unique solutions and validate positivity and boundedness, the Banach contraction principle was applied. Asthma disease transmission among smokers was evaluated using the fundamental reproductive number (R_0). The study also examined the sensitivity of the reproductive number and established equilibrium points. Techniques for chaos control were used to manage the spread of the illness. The global stability of equilibrium points was validated by the Lyapunov function. Numerical simulations were used to illustrate the model's usefulness and show how it improved efficiency at different fractional orders. Our results confirm the significance of non-local Caputo derivatives in modeling for respiratory diseases such as asthma, where the memory effect is crucial. We found that asthma disease grows with greater fractional orders (θ), whereas asthma propagates considerably more slowly with smaller values of θ. These results aid in understanding the effects of asthma through public health initiatives. We can therefore conclude that our suggested model will support sophisticated mathematical modeling to investigate the dynamics of additional long-term respiratory conditions. According to the study, working with public health specialists and utilizing actual data on asthma might help policymakers better comprehend the problem at hand and create efficient disease management measures. In order to improve resource allocation tactics and get a deeper understanding of disease dynamics, further studies should investigate how the model can be applied under other differential operators and incorporate fractional derivatives using machine learning approaches.

The suggested model ignores natural demographic shifts and other environmental triggers and is based on the supposition that smoking is the main factor influencing asthma dynamics in a population. Predictive accuracy may be limited by the literature-based parameters that were employed. In order to evaluate the effects of different memory kernels on the progression of asthma, future research may concentrate on applying optimal control techniques for assessing smoking cessation policies and expanding the framework by comparing different fractional operators, such as Caputo-Fabrizio and Atangana-Baleanu derivatives.

Acknowledgement: None.

Funding Statement: This research received no external funding.

Author Contributions: The contributions of each author to this research are as follows: Conceptualization, Muhammad Farman, Noreen Asghar and Kottakkaran Sooppy Nisar; methodology, Muhammad Farman, Noreen Asghar and Muhammad Umer Saleem; software, Noreen Asghar and Muhammad Umer Saleem; validation, Kamyar Hosseini and Mohamed Hafez; formal analysis, Muhammad Umer Saleem; investigation, Muhammad Farman, Muhammad Umer Saleem and Kottakkaran Sooppy Nisar; resources, Kamyar Hosseini; data curation, Mohamed Hafez; writing—original draft preparation, Muhammad Farman and Noreen Asghar; writing—review and editing, Muhammad Farman, Noreen Asghar, Muhammad Umer Saleem, Kottakkaran Sooppy Nisar; visualization, Muhammad Farman and Kottakkaran Sooppy Nisar; supervision, Kamyar Hosseini and Mohamed Hafez; project administration, Muhammad Farman. All authors reviewed the results and approved the final version of the manuscript.

Availability of Data and Materials: All data analyzed and generated during this study are included in this article.

Ethics Approval: Not applicable.

Conflicts of Interest: The authors declare no conflicts of interest to report regarding the present study.

References

1. Ghosh M. Industrial pollution and Asthma: a mathematical model. J Biolog Syst. 2000;8(4):347–71. doi:10.1142/s0218339000000225.
2. Polosa R, Thomson NC. Smoking and asthma: dangerous liaisons. Eur Respir J. 2013;41(3):716–26. doi:10.1183/09031936.00073312.
3. Strachan DP. The role of environmental factors in asthma. Br Med Bull. 2000;56(4):865–82. doi:10.1258/0007142001903562.
4. Driscoll AJ, Arshad SH, Bont L, Brunwasser SM, Cherian T, Englund JA, et al. Does respiratory syncytial virus lower respiratory illness in early life cause recurrent wheeze of early childhood and asthma? Critical review of the evidence and guidance for future studies from a World Health Organization-sponsored meeting. Vaccine. 2020;38(11):2435–48. doi:10.1016/j.vaccine.2020.01.020.
5. Canadian Medical Association. Secondhand cigarette smoke worsens symptoms in children with asthma. Section on Allergy, Canadian Paediatric Society. CMAJ. 1986;135(4):321–3.
6. Collishaw NE, Kirkbride J, Wigle DT. Tobacco smoke in the workplace: an occupational health hazard. Can Med Assoc J. 1984;131(10):1199.
7. Dockery DW, Pope CA, Xu X, Spengler JD, Ware JH, Fay ME, et al. An association between air pollution and mortality in six US cities. New Engl J Med. 1993;329(24):1753–9. doi:10.1056/nejm199312093292401.
8. Utell MJ, Looney RJ. Environmentally induced asthma. Toxicol Lett. 1995;82:47–53. doi:10.1016/0378-4274(95)03467-6.
9. Jan R, Xiao Y. Effect of partial immunity on transmission dynamics of dengue disease with optimal control. Math Methods Appl Sci. 2019;42(6):1967–83. doi:10.1002/mma.5491.
10. Akinyemi ST, Idisi IO, Rabiu M, Okeowo VI, Iheonu N, Dansu EJ, et al. A tale of two countries: optimal control and cost-effectiveness analysis of monkeypox disease in Germany and Nigeria. Healthcare Analytics. 2023;4:100258. doi:10.1016/j.health.2023.100258.
11. Sohaib M. Mathematical modeling and numerical simulation of HIV infection model. Res Appl Mathem. 2020;7(41):100118. doi:10.1016/j.rinam.2020.100118.
12. Attaullah RJ, Jabeen A. Solution of the HIV infection model with full logistic proliferation and variable source term using Galerkin scheme. Matrix Science Mathematic. 2020;4(2):37–43. doi:10.26480/msmk.02.2020.37.43.
13. Jan R, Xiao Y. Effect of pulse vaccination on dynamics of dengue with periodic transmission functions. Adv Differ Equ. 2019;2019(1):1–17.
14. Mahmoudi MR, Baleanu D, Band SS, Mosavi A. Factor analysis approach to classify COVID-19 datasets in several regions. Results Phys. 2021;25:104071. doi:10.1016/j.rinp.2021.104071.
15. Baskonus HM, Hammouch Z, Mekkaoui T, Bulut H. Chaos in the fractional order logistic delay system: circuit realization and synchronization. AIP Conf Proc. 2016;1738(1):290005. doi:10.1063/1.4952077.
16. Slowikowska M, Bajzert J, Miller J, Stefaniak T, Niedzwiedz A. The dynamics of circulating immune complexes in horses with severe equine asthma. Animals. 2021;11(4):1001. doi:10.3390/ani11041001.
17. Khan D, Ali G, Khan ZA. Heat transfer capability analysis of hybrid Brinkman-type fluid on horizontal solar collector plate through fractal fractional operator. Opt Quantum Electron. 2025;57(2):154. doi:10.1007/s11082-024-08025-8.
18. Farman M, Xu C, Shehzad A, Akgül A. Modeling and dynamics of measles via fractional differential operator of singular and non-singular kernels. Math Comput Simul. 2024;221(1):461–88. doi:10.1016/j.matcom.2024.03.019.
19. Mohamed Hafez, Faisal Alshowaikh, Betty Wan Niu Voon, Shawkat Alkhazaleh, Hussein Al-Faiz. Review on recent advances in fractional differentiation and its applications. Progr Fract Differ Appl. 2025;11(2):245–261. doi:10.18576/pfda/110203.
20. Awadallah M, Hannabou M, Zaway H, Alahmadi J. Applicability of Caputo-Hadmard fractional operator in mathematical modeling of pantograph systems. J Appl Math Comput. 2025;71:4971–86. doi:10.1007/s12190-025-02421-3.

21. Farman M, Nisar KS, Shehzad A, Baleanu D, Amjad A, Sultan F. Computational analysis and chaos control of the fractional order syphilis disease model through modeling. Ain Shams Eng J. 2024;15(6):102743. doi:10.1016/j.asej.2024.102743.
22. Madani YA, Ali Z, Rabih M, Alsulami A, Eljaneid NH, Aldwoah K, et al. Discrete fractional-order modeling of recurrent childhood diseases using the caputo difference operator. Fract Fraction. 2025;9(1):55. doi:10.3390/fractalfract9010055.
23. Farman M, Akgül A, Conejero JA, Shehzad A, Nisar KS, Baleanu D. Analytical study of a Hepatitis B epidemic model using a discrete generalized nonsingular kernel. AIMS Math. 2024;9(7):16966–97. doi:10.3934/math.2024824.
24. Matouk AE, Botros M. Hidden chaotic attractors and self-excited chaotic attractors in a novel circuit system via Grünwald-Letnikov, Caputo-Fabrizio and Atangana-Baleanu fractional operators. Alex Eng J. 2025;116(2):525–34. doi:10.1016/j.aej.2024.12.064.
25. Dinku T, Kumsa B, Rana J. A mathematical approach to cancer growth: the role of smoking through fractional order models with Mittag-Leffler kernels. Alex Eng J. 2025;124(4):46–65. doi:10.1016/j.aej.2025.03.013.
26. Ferrari AL, Gomes MCS, Aranha ACR, Paschoal SM, de Souza Matias G, de Matos Jorge LM, et al. Mathematical modeling by fractional calculus applied to separation processes. Sep Purif Technol. 2024;337:126310. doi:10.1016/j.seppur.2024.126310.
27. Nisar KS, Kulachi MO, Ahmad A, Farman M, Saqib M, Saleem MU. Fractional order cancer model infection in human with CD8+ T cells and anti-PD-L1 therapy: simulations and control strategy. Sci Rep. 2024;14(1):16257. doi:10.1038/s41598-024-66593-x.
28. Mukhtar R, Chang CY, Raja MAZ, Chaudhary NI, Shu CM. Novel nonlinear fractional order Parkinson's disease model for brain electrical activity rhythms: intelligent adaptive Bayesian networks. Chaos Soliton Fract. 2024;180:114557. doi:10.1016/j.chaos.2024.114557.
29. Sun L, Cheng G, Barriere T. Investigation of temperature-dependent mechanical behaviours of polycarbonate with an innovative fractional order model. Mat Res Proc. 2024;41:2174–81. doi:10.21741/9781644903131-239.
30. Farman M, Jamil K, Xu C, Nisar KS, Amjad A. Fractional order forestry resource conservation model featuring chaos control and simulations for toxin activity and human-caused fire through modified ABC operator. Math Comput Simul. 2025;227(2):282–302. doi:10.1016/j.matcom.2024.07.038.
31. Adak S, Barman S, Jana S, Majee S, Kar TK. Modelling and analysis of a fractional-order epidemic model incorporating genetic algorithm-based optimization. J Appl Math Comput. 2025;71(1):901–25. doi:10.1007/s12190-024-02224-y.
32. Bansal J, Kumar A, Kumar A, Khan A, Abdeljawad T. Investigation of monkeypox disease transmission with vaccination effects using fractional order mathematical model under Atangana-Baleanu Caputo derivative. Model Earth Syst Environ. 2025;11(1):40. doi:10.1007/s40808-024-02202-0.
33. Naresha R, Tripathi A. A nonlinear mathematical model for asthma: effect of environmental pollution. Iranian J Optimizat. 2009;1:24–56.
34. Jan R, Yüzbaşi S, Attaullah A, Jawad M, Jan A. Fractional derivative analysis of asthma with the effect of environmental factors. Sigma J Eng Nat Sci. 2024;42(1):177–88. doi:10.14744/sigma.2023.00098.
35. Tuza FADA, de Sá PM, Castro HA, Lopes AJ, de Melo PL. Combined forced oscillation and fractional-order modeling in patients with work-related asthma: a case-control study analyzing respiratory biomechanics and diagnostic accuracy. Biomed Eng Online. 2020;19:1–30. doi:10.21203/rs.3.rs-31314/v2.
36. Padder A, Almutairi L, Qureshi S, Soomro A, Afroz A, Hincal E, et al. Dynamical analysis of generalized tumor model with Caputo fractional-order derivative. Fract Fraction. 2023;7(3):258. doi:10.3390/fractalfract7030258.